UNIVERSIDADE DA BEIRA INTERIOR

Ciências da Saúde

Desenvolvimento de Scaffolds para futura aplicação na Regeneração Óssea

Inês Raquel Tavares Serra

Dissertação para obtenção do Grau de Mestre em

Ciências Biomédicas

(2º ciclo de estudos)

Orientador: Prof. Doutor Ilídio Joaquim Sobreira Correia

Covilhã, Outubro de 2013

List of Publications

Torres, A., Gaspar, V., Serra, I., Diogo, G., Fradique, R., Silva, A. and Correia, I.; Bioactive polymeric-ceramic hybrid 3D scaffold for application in bone tissue regeneration. Materials Science and Engineering: C. (2013). **33** (7): 4460-4469.

“O sucesso é a soma de pequenos esforços repetidos dia após dia.”

(Robert Collier)

Acknowledgments

At the end of another stage of my life, I want to thank all those who, in one way or another, contributed for reaching this stage of my life.

Firstly, I would like to express my gratitude to my supervisor Professor Ilídio Correia, for the opportunity to develop this project and for all the support, patience and guidance during this Master Thesis.

I would like to thank the Eng. Ana Paula from the Optics Department of the University of Beira Interior, for the time that she spent on the acquisition of the scanning electron microscopy images.

I also acknowledge to Professor Abílio Silva from the Department of Electrochemical Engineering of the University of Beira Interior, for their availability in carrying out the mechanical assays.

To my group colleagues, I would thank for everything. Thanks for all the help, support and courage. A special thanks to Gabriela, who has been present in every moments during this year. Thanks for all the support, help and especially the patience during the year. To Paulo thanks for all the help.

To my closest friends thanks for all good moments they that provided me over the years. For all courage, love and support in moments less good, they have given me and for never let me give up. A special thanks to my best friend Ana Raquel Nunes, for all the support, not only at the professional level but also personal. Thanks for never having stopped believe in me!

Lastly, but no less importantly, thank you to my father and my mother. First, the financial support that they provide me over these five years. But even more important for all the dedication, support, love and patience. Thanks also to my sister, coined and goddaughter all the force and support. Thank you for never stopped to believe in me.

Without you, none of this would be possible!

Abstract

Bone is the main component of the human skeleton. This tissue is responsible for several functions at the structural and biological level. It is a tissue that is highly vascularized and dynamic, with excellent mechanical properties and also has the capacity for self-regeneration. However, several factors as aging, disorders at metabolic level and fractures, can lead to a loss of integrity of this tissue. In this context, it is necessary to develop bone substitutes that mimic the structure of extracellular matrix and induce regeneration of the damaged tissue. Currently, the most commonly clinical treatments used are based in the application of bone grafts obtained from the patient or from another. However, these therapeutic approaches present several limitations, namely immunologic responses and infectious risks. Tissue Engineering, an area that aims to develop biological substitutes that are able to enhance, restore or replace the damaged tissue, has emerged as an area of research that is looking for new solutions to improve bone regeneration. In this field of research, several types of biomaterials have been developed for this purpose. Among these, three dimensional structures, also known as scaffolds are the most promising because these structures possess the essential properties needed for the bone regeneration, such as biocompatibility, biodegradability and porosity. Besides, scaffolds provide a structure that mimic extracellular matrix which is fundamental to promote cell adhesion and proliferation until tissue regeneration occurs. In this context, novel biomaterials based in chitosan, gelatin and beta-tricalcium phosphate were developed in this work, in order to be applied in a near future in bone regeneration. Several physical-chemical and mechanical studies were performed, to study the influence of the incorporation of gelatin and beta tricalcium phosphate in the structure of chitosan scaffolds. Besides, biological studies were performed in vitro with human osteoblasts to evaluate the materials cytotoxic profile. The results obtained demonstrate that the scaffolds developed provide a suitable support for cell adhesion and proliferation. Moreover, the scaffolds do not present toxicity, highlighting its application in regenerative medicine.

Keywords:

Beta Tricalcium Phosphate, Bone Remodeling, Chitosan, Gelatin, Scaffolds.

Resumo

O osso é o principal componente do esqueleto humano, desempenhando diversas funções a nível estrutural e biológico. É um tecido altamente vascularizado e dinâmico, com propriedades mecânicas excepcionas e com capacidade de se auto-regenerar ao longo da vida. No entanto, existem diversos factores como o envelhecimento, desordens a nível metabólico e fraturas, que podem levar à perda da integridade deste tecido. Neste contexto, surge a necessidade de desenvolver substitutos ósseos que mimetizem a sua estrutura e induzam a sua regeneração. Atualmente, os tratamentos clínicos mais usados baseiam-se na aplicação de enxertos ósseos do próprio paciente ou proveniente de outro. Contudo, estas abordagens terapêuticas apresentam diversas desvantagens para o paciente, nomeadamente riscos imunológicos e de transmissão de doenças. De forma a colmatar estas limitações, surge a Engenharia de Tecidos, uma área de investigação que tem procurado desenvolver novos substitutos biológicos que possuam a capacidade de melhorar, restaurar ou mesmo substituir o tecido lesado. Com este intuito, têm sido desenvolvidos vários tipos de biomateriais. Neste campo, estruturas tridimensionais, também conhecidas como *scaffolds*, revelam ser os mais promissores. Estes possuem propriedades essenciais no processo de regeneração óssea, tais como biocompatibilidade, biodegradabilidade e porosidade. Simultaneamente, estas estruturas tridimensionais permitem a criação de uma estrutura com a capacidade de mimetizar a matriz extracelular, e desta forma favorecer a adesão e proliferação celular até ocorrer a regeneração do tecido lesado. Neste contexto, novos biomateriais a base de quitosano, gelatina e beta fosfato tricálcico, foram desenvolvidos ao longo deste trabalho, para futura aplicação na regeneração óssea. Vários estudos das propriedades físico-químicas e mecânicas dos materiais foram realizados com o objectivo de estudar qual a influência da incorporação da gelatina e do beta fosfato tricálcico em *scaffolds* de quitosano. Além disso, o perfil citotóxico dos materiais foi caracterizado *in vitro*, através da utilização de osteoblastos humanos. Os resultados obtidos demonstram que as estruturas desenvolvidas fornecem um suporte adequado à adesão e proliferação celular. Além disso, não apresentam efeitos tóxicos para as células, evidenciando a sua possível aplicação na área da medicina regenerativa.

Palavras-chave:

Andaimes, Beta Fosfato Tricálcico, Gelatina, Quitosano, Regeneração Óssea.

Resumo Alargado

O osso é o principal componente do esqueleto humano, desempenhando várias funções altamente especializadas. A nível mecânico é responsável pelo suporte e locomoção do corpo, e confere protecção de alguns órgãos, como o coração e os pulmões. A nível biológico está envolvido na produção de células sanguíneas e no armazenamento de iões, essencialmente cálcio e fosfato. É um tecido dinâmico e altamente vascularizado com capacidade de regeneração intrínseca, o que possibilita a sua constante substituição por tecido novo, assegurando desta forma a sua integridade. No entanto, existem inúmeros factores que comprometem a sua integridade: a medida que o indivíduo envelhece ocorre um decréscimo da densidade óssea, o que torna o osso mais suscetível a fraturas; bem como as forças a que o osso está sujeito diariamente, muitas vezes superiores àquelas que ele suporta, podendo resultar em fraturas graves que acabam por afetar a qualidade de vida do paciente. Nestas situações, é necessário que o mecanismo de remodelação óssea ocorra de forma natural. O processo de remodelação do osso ocorre em duas fases bastante distintas: fase de reabsorção e fase de formação, entre as quais deve existir sempre um balanço que permita uma coordenação efetiva entre os diversos eventos celulares e moleculares, que ocorrem neste processo. No entanto, em traumatismos ósseos graves que envolvam múltiplas fraturas, tumores ósseos e desordens a nível metabólico, onde a integridade do tecido é afetada, a capacidade de auto-remodelação torna-se limitada. Neste contexto, surge a necessidade de desenvolver substitutos ósseos que mimetizem a sua estrutura e promovam a sua regeneração, sem causar qualquer rejeição por parte do paciente. Atualmente, as abordagens terapêuticas mais usadas são os auto-enxertos, alo-enxertos e xeno-enxertos. Os auto-enxertos, enxertos de osso provenientes do próprio paciente, não apresentam qualquer risco imunológico, contudo são limitados para grandes defeitos ósseos. Por outro lado, alo-enxertos e xeno-enxertos, enxertos do osso obtidos de outro paciente da mesma espécie ou de diferentes espécies, respetivamente, podem causar rejeição pelo organismo do paciente. Com o intuito de colmatar estas limitações vários investigadores têm tentado desenvolver o substituto ósseo ideal, surgindo assim uma nova área de pesquisa, a Engenharia de Tecidos. A Engenharia de Tecidos combina os conhecimentos da engenharia e das ciências da vida e visa o desenvolvimento de substitutos biológicos que possuam a capacidade de melhorar, restaurar ou mesmo substituir o tecido lesado. Vários tipos de biomateriais como próteses, substratos injetáveis e hidrogéis têm sido desenvolvidos com esta finalidade. Neste campo, estruturas tridimensionais, também conhecidas como *scaffolds*, revelam ser as mais promissoras pois possuem propriedades essenciais para o processo de regeneração óssea, tais como biocompatibilidade, biodegradabilidade e porosidade. Além disso, promovem uma estrutura que mimetiza a matriz extracelular favorecendo a adesão e proliferação celular até ocorrer a regeneração do tecido lesado. Para a produção destas estruturas tridimensionais têm sido utilizados vários tipos de materiais e diversos métodos. Estes fatores tornam-se fulcrais, pois

a aplicação em tecidos biológicos dos *scaffolds* produzidos exige que os mesmos sejam produzidos com biomateriais que não desencadeiem nenhuma resposta inflamatória nem comprometam a viabilidade do tecido em contacto com o material. Neste âmbito, têm sido usados vários métodos tradicionais como o processamento a alta pressão, lixiviação de partículas, contudo, apresentam toxicidade devido ao uso de solventes orgânicos, baixa resistência mecânica e estruturas não porosas, o que os torna inadequados para a regeneração do tecido ósseo. Assim, para eliminar alguns destes problemas têm sido usados métodos que envolvem a criopreservação das amostras, permitindo a criação de estruturas altamente porosas e sem qualquer toxicidade.

Neste contexto, *scaffolds* produzidos com materiais biocompatíveis neste estudo foram desenvolvidos, para futura aplicação na regeneração óssea, utilizando quitosano, gelatina e beta fosfato tricálcico. Vários estudos das propriedades físico-químicas e mecânicas dos materiais foram realizados com o objectivo de estudar qual a influência da incorporação da gelatina e do beta fosfato tricálcico em *scaffolds* de quitosano. Além disso, o perfil citotóxico dos materiais foi caraterizado *in vitro*, através da utilização de osteoblastos humanos. Os resultados obtidos demonstram que as estruturas desenvolvidas fornecem um suporte adequado à adesão e proliferação celular. Além disso, não apresentam efeitos tóxicos para as células, evidenciando a sua possível aplicação na área da medicina regenerativa.

Index

List of Figures

List of Tables

List of Acronyms

3D	Three-Dimensional
BMP	Bone Morphogenic Factors
ß-TCP	Beta Tricalcium Phosphate
BSA	Bovine Serum Albumin
CH	Chitosan
DMEM-F12	Dulbecco's Modified Eagle's Medium
ECM	Extracellular Cellular Matrix
EDS	Energy Dispersive Spectroscopy
EDTA	Ethylenediaminetetraacetic Acid
FBS	Fetal Bovine Serum
FTIR	Fourier Transform Infrared Spectroscopy
GAGs	Glycosaminoglycans
GEL	Gelatin
HA	Hydroxyapatite
IGF-II	Insulin-Like Growth Factor II
M-CSF	Macrophage Colony-Stimulating
MMPs	Matrix Metalloproteinases
MSC	Mesenchymal Stem Cells
MTS	3-(4,5-dimethylthiazol-2-yl)-5-(3-carboxymethoxyphenyl)-2-(4-sulfophenyl)-2H-Tetrazolium Reagent, Inner Salt
NAOH	Sodium Hydroxide

PBS	Phosphate Buffered Saline
OB	Osteoblasts
OC	Osteoclasts
PTH	Parathyroid Hormone
RANK	Receptor Activator for Nuclear Factor K B
RANKL	Receptor Activator for Nuclear Factor K B Ligand
RER	Rough Endoplasmatic Reticulum
RT	Room Temperature
SEM	Scanning Electronic Microscopy
TCPS	Tissue Culture Polystyrene
TE	Tissue Engineering
TGF	Transforming Growth Factor
TPP	Sodium Tripolyphosphate
XRD	X-Ray Diffraction

Chapter I
Introduction

1. Introduction

1.1. Bone Tissue

Bone is a dense tissue that is the main component of human skeleton. It is composed by bone matrix, cells and water and it is involved in various functions (1). Bone is responsible for supporting the weight and locomotion of the entire body. Besides, it also confers protection to some organs, such as the heart and lungs. Moreover, it acts as storage of minerals like calcium and phosphorous ions, and produces blood cells through hematopoiesis (2).

1.1.1. Types of bone

The human bones can be classified in different classes, depending on the shape, on the relation between the amount of bone matrix and spaces present and on the organization of the collagen fibres within bone matrix (2).
Relying on shape and size, bone can be classified into long, short, flat or irregular (Table 1).

Table 1: Bone classification according to shape (Adapted from (2, 3)).

Bone Classification	Features	Functions	Examples
Long	Cylinder-like shape	Leverage	Femur, tibia, fibula, humerus, radius
Short	Cube-like shape	Stability and Support	Carpals, tarsals
Flat	Thin and curved	Points of attachment for muscles; protectors of internal organs;	Sternum, ribs and cranial bones
Irregular	Complex shape	Protect internal organs	Vertebrae and facial bones

The long bones are constituted by three main components: diaphysis, epiphysis and epiphyseal plate, as shown in Figure 1. The epiphysis, present at the end of the bone, is constituted by spongy bone, composed by small cavities surrounded by bone matrix. The diaphysis is between the distal and proximal epiphysis, being formed by compact bone, consisting mostly of bone matrix. Besides these cavities, the diaphysis has a cavity of great biological interest, the medullary cavity, which is filled with bone marrow that is responsible

for the production of blood cells (red marrow) and storage of a large amount of adipose tissue (yellow marrow). These structures are separated by the epiphyseal plate.

In addition to these structures, bone also contains the periosteum and endosteum. The periosteum is a membrane that covers the outer surface of the bone and it is composed by two layers. The outer layer is formed by collagen-rich tissue and blood vessels. The inner one is composed by a layer of bone cells. The endosteum has only on layer of cells and coats all surfaces of the bone cavity, such as medullary cavity (Figure 1) (2).

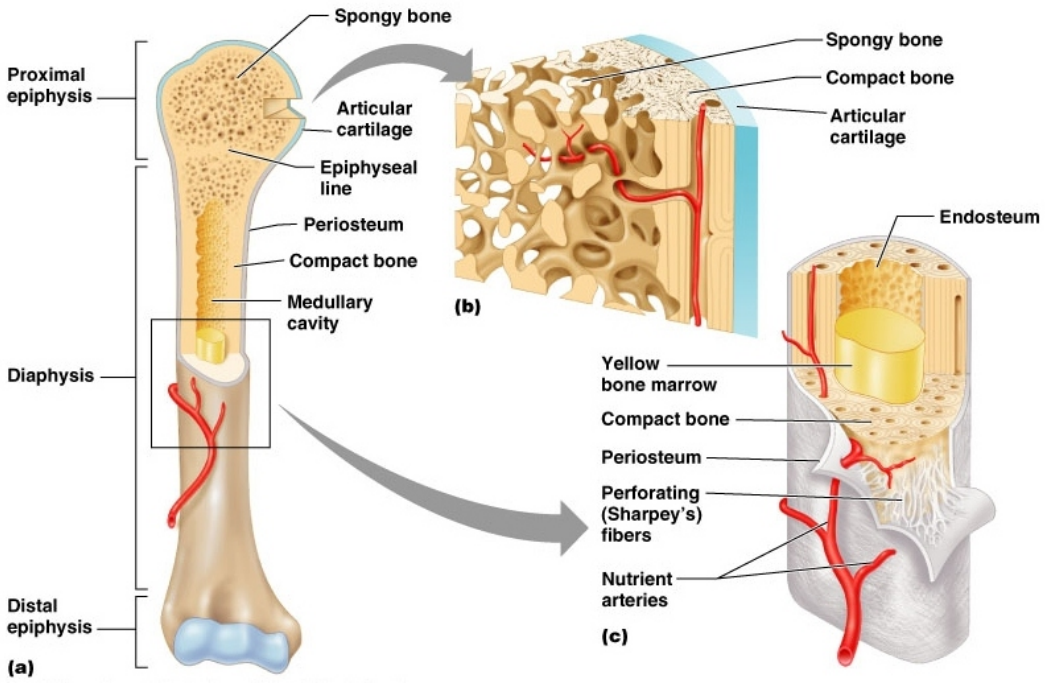

Figure 1: Representation of the anatomy of a long bone. a) Anterior view of the bone. b) Spongy and compact bone in the epiphysis region of the bone. c) Cross-sectional view of the diaphysis of bone (Adapted from (4)).

According to density, bone can be classified into trabecular (or cancellous) and cortical (or compact) bone, as shown in Figure 1 (3). Trabecular bone is the first to be formed during the foetal development or after a fracture occur and it represents 20% of the total skeleton. It is arranged in a sponge-like pattern, with high porosity and has a high number of blood vessels. Furthemore, it is present in regions where bone is subjected to compression. The cortical bone has a greater density, lower porosity and lower number of blood vessels in comparison to trabecular bone. This type of bone is involved mainly in tension, compression and torsion. The mechanical properties of trabecular and cortical bone are presented in Table 2 (5).

Table 2: Mechanical properties of cortical and spongy bone (Adapted from (5)).

Properties	Measurements	
	Cortical bone	Trabecular bone
Young´s modulus /GPa	14-20	0.05-0.5
Tensile Strength/MPa	50-150	10-20
Compressive Strength/MPa	170-193	7-10
Fracture toughness / (MPa.m$^{1/2}$)	2-12	0.1
Density / (g.cm^3)	18-22	0.1-1.0
Porosity %	10%	50-90 %

Finally, based on collagen fibres organization within the matrix, bone can be classified in reticular or lamellar. The reticular bone is the first to be formed in foetal development or repair, in case facture. This is characterized by containing the collagen fibres distributed randomly in various directions. The lamellar bone is a mature bone arranged in thin layers (lamellae), where the collagen fibres are arranged in parallel (2).

1.1.2. Bone Matrix

Like other connective tissues, bone is made of cells and extracellular matrix (ECM). ECM is composed of an organic (35%) and inorganic phase (65%) (1, 2). The organic phase, known as osteoid, is constituted mainly by type I collagen, being responsible for conferring elasticity to bone, and 5 % non-collagenous components (3, 4). The non-collagenous components include matrix proteins (osteocalcin, osteopontin and osteonectin), growth factors like transforming growth factor (TGF-ß), cytocines such as macrophage colony-stimulating factor (M-CSF) and nuclear factor-Kß ligand (RANK) receptor activator. The main function performed by these non-collagenous components is to regulate the activity of bone cells in the bone remodelling process, mediating the binding of these cells to bone matrix (6). Regarding the inorganic phase, it is mainly formed by phosphate and calcium ions, deposited as hydroxyapatite (HA) crystals that are responsible for conferring resistance of bone (2).

To ensure the integrity of the bone it is necessary the maintenance of an equilibrium between the two phases. If the bone is only constituted by the organic phase, it becomes far too flexible. On the other hand, if the collagen reaches low concentration the bone becomes fragile and brittle (2).

1.1.3. Bone Cells

Bone is formed by three cell types, namely, osteoblasts (OB), osteocytes and osteoclasts (OC) that have different origins and functions (Figure 2).

OB are mononuclear cells that derive from Mesenchymal Stem Cells (MSC) (7). Structurally, these cells have large and spherical nucleus presenting high number of Rough Endoplasmic Reticulum (RER), Golgi apparatus, and mitochondria. OB are involved in the formation of the bone matrix, being responsible for the production of collagen type I and non-collagenous proteins. Moreover, OB contains alkaline phosphatase (ALP) that contributes for bone mineralization (8).

After bone matrix formation be performed by osteoblastic cells, the matrix that is being produced surrounded the OB and they subsequently differentiate into mature cells, called osteocytes, which are the most abundant cells in bone tissue. These cells present stellar shape and, compared to OB, have a lower number of organelles involved in synthesis and secretion, such as RER and Golgi apparatus. However, osteocytes are essential to maintain bone homeostasis, since they regulate the levels of calcium and phosphorus in this tissue (8).

Finally, OC are multinucleated cells derived from haematopoietic cells of the macrophage lineage (9). Those cells are involved essentially in bone reabsorption during growth and bone remodelling, getting in contact with the bone matrix and forming an area called ruffled border. This area assumes great importance because it is through it that OC release hydrogen ions that create an acidic environment and subsequently degrade bone matrix (10). Moreover, OC have the ability to connect with other osteocytes and even with OB, allowing the detection of bone alterations and its communication to neighbouring OB and OC.

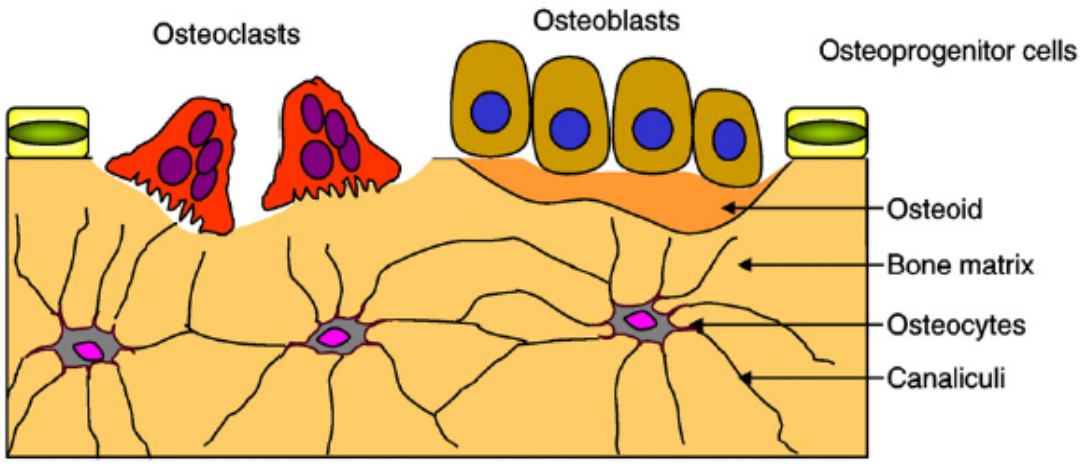

Figure 2: Bone structure at cellular level (Adapted from (11)).

1.1.4. Bone Remodeling

Bone is a dynamic tissue that is under the active control of both bone-forming OB and bone-resorbing OC. Aiming to sustain bone integrity and also in extreme situations that lead to bone injury, bone tissue remodeling is fundamental. The remodeling process of bone comprises four main stages: quiescence, resorption, reversal and formation phase, as shown in Figure 3.

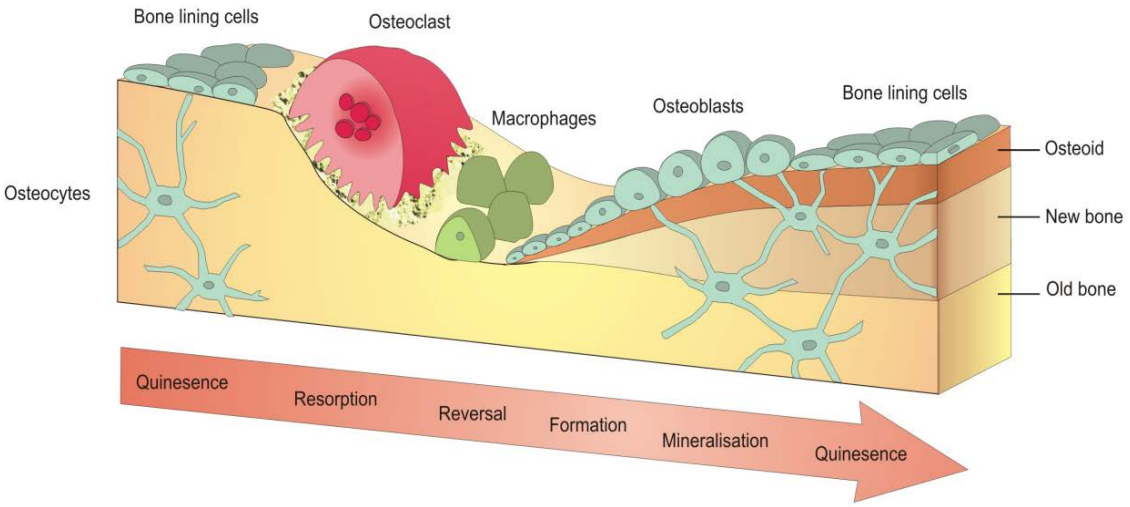

Figure 3: Representation of a bone remodeling cycle (Adapted from (12)).

Quiescence Phase: This phase involves an initial signal that can be, for instance the detection of damage in the bone structure or the presence of hormones such as Parathyroid Hormone (PTH) (13). On a daily basis this tissue is subjected to different forces, which sometimes can be higher than those that bone can support, resulting in bone tissue damage. When this happens, osteocytes detect these changes and translate them into biological signals that initiate the bone tissue remodeling process. Then, the osteoclastogenesis rate increases and consequently the onset bone resorption phase. On the other hand, PTH can also induce bone resorption by OC. PTH is secreted by the parathyroid glands in response to a reduction of serum calcium, being thus involved in the maintenance of calcium homeostasis. Thus, the decrease of calcium levels in serum leads to a significant increase of the PTH hormone activity. This hormone binds to receptors present in osteoblastic cells, leading these to produce Receptor Activator for nuclear factor K B ligand (RANKL) that subsequently binds to its receptor RANK present in OC surface, activating this cell type (14, 15).

Resorption Phase: The precursors of osteoclasts are attracted to the injury site, and become differentiated into mature OC. This differentiation requires the action of two major, cytokines that are released from OB, M-CSF and RANKL. M-CSF is involved mainly in the proliferation and survival of OC precursors, while RANKL promotes the proliferation of OC precursors (10). Subsequently, mature OC adhere to bone surface by integrins avβ3. Thus, OC resorb bone by secreting hydrochloric acid and proteolytic enzimes, through ruffled border. Hydrochloric acid dissolves hydroxyapatite and allows proteolitic enzymes, essentially cathepsin K to degrade components (mainly collagen) of the bone matrix (16, 17).

Reversal phase: When OC complete the resorption process, they migrate from the surface of bone and undergo programmed cell death (apoptosis), in a stage called reversal phase. This phase begins the process of bone formation (6).

Formation Phase: The precursors of OB are attracted to the area where bone was resorbed and become differentiated into OB. As previously described, they have in its constitution type I collagen, osteocalcin and ALP enzyme that are involved in the production of the new matrix. In the last osteoid phase, bone formation stops and following bone mineralization, bone lining cells remains in a quiescent state (18).

To ensure the health of the bone tissue it is essential that the process of bone remodeling occurs correctly. There is a balance between bone formation and bone resorption, as shown in Figure 4.

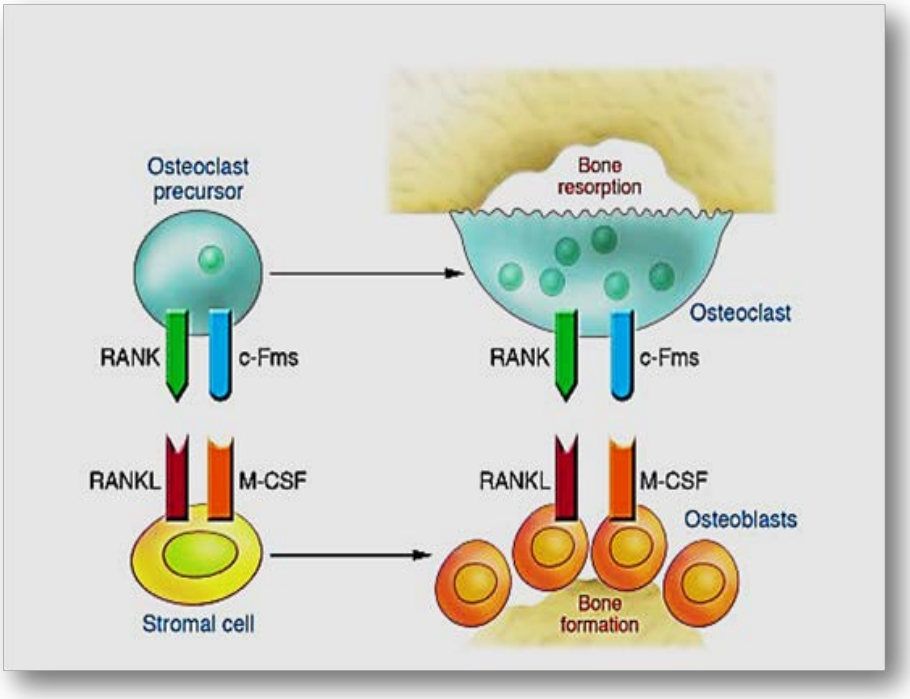

Figure 4: Balance between bone formation and bone resorption (Adapted from (19)).

1.2. Bone Disorders

As previously described, to ensure that the bone remodeling process occurs normally, it is necessary a tight coupling between bone resorption and bone formation. However, factors like ageing, physiological changes (e.g., menopause and diseases) can cause changes in bone remodeling cycle and subsequently allow the development of bone disorders like Osteoporosis, Osteomalacia and Paget´s diseases (20).

Osteoporosis is characterized by a reduction of the amount of bone density, which occurs when the rate of bone resorption exceeds bone formation, making bones more fragile and subsequently increasing the risk of fracture (21). A variety of factors may be responsible for this disorder. One of the main factors that can lead to decrease of bone mass in both sexes is ageing. During adolescence, bones are in development and growth, reaching the peak bone mass in adulthood. In this phase the amount of bone formed is higher than the amount reabsorbed. However, bone mass begins to decrease after 35 years of age, due to decreased levels of calcium in the blood. Moreover, in the case of women, the menopause can also lead to a decrease in bone mass. This happens due to a reduction of the estrogens released from the ovaries. Since, they are responsible for the maintenance of the bone mass at normal values through the inhibition of PTH and subsequently the inhibition of OC activity. However, at post-menopausal phase the amount of estrogens decrease leading to an increased activity of the PTH and subsequently, to an increase activity of the OC. Lastly, the increase of glucocorticoid (GC) level in blood, use in the treatment of inflammatory and autoimmune diseases, can also lead to development of osteoporosis (22).

Osteomalacia is characterized by impaired mineralization of bone, increasing its flexibility and consequently causing its deformation. The main factor involved in this disorder is the insufficiency of vitamin D, due to a poor diet in this vitamin or insufficient exposure to sunlight. So, for bone grow normally it is essential that the body absorb calcium and phosphorus ions correctly. However, for a correct absorption of these ions it is necessary the presence of sufficient quantities of vitamin D. When this vitamin is present in insufficient quantities in the organism, it loses the ability to properly absorb calcium and phosphorous ions, resulting in abnormal bone growth (21).

Paget´s disease is defined by excessive and haphazard bone resorption and formation, leading to structural defects that cause bone pain and deformity. Although, the factors associated with this disorder are not yet well understood, changes in diet, exposure to infections, mechanical loading of the skeleton are considered risk factors (12).

1.3. Bone Grafts

Bone has the ability to self-remodeling over life, however, due to injury or traumas it is the second most common transplanted tissue (23). Every years, millions of people are suffering from bone defects due to trauma, tumors and bony diseases that in some cases may lead to death (24). To avoid such situations, it is necessary to find an ideal bone substitute that promotes bone remodeling. Three different types of bone grafts are currently available and have been used in the majority of the cases: autografts, allografts and xenografts (25). Autografts are the most used grafts and are obtained from other parts of the patient´s body. However, these grafts present several disadvantages. The implantation of these grafts requires that patients are submitted to surgery, which may lead to a long recovery for patients, increasing the risk of infection. Moreover, the use of autografts is limited to large bone defects (26, 27). On the other hand, allografts and xenografts consist in the transplantation from other individuals, from the same or different species, respectively. However, these grafts can cause immune rejection by patients or be responsible for transmission of diseases (28).

1.4. Tissue Engineering

As previously described, when a bone defects occur it is necessary to develop substitutes that can replace the function of the damaged bone tissue. In order to overcome the drawbacks associated with autografts, allografts and xenografts, it is necessary to develop new bone substitutes. In this context, arise a new and revolutionary area called Tissue Engineering (TE). As it was defined by Langer and Vacanti, TE is ‘‘an interdisciplinary field of research that applies the principles of engineering and the life sciences towards the development of biological substitutes that restore, maintain, or improve tissue function’’ (29).

Specifically, TE for bone regeneration is focused on the development of alternatives to replace the injured bone tissue, in order to promote bone regeneration without causing immune rejection on the patient (30).

1.4.1. Scaffolds for bone regeneration

Bone Tissue Engineering is based on developing three-dimensional (3D) structures, commonly known as scaffolds that promote bone regeneration. Scaffolds are three-dimensional matrices that act as temporary templates for cell adhesion and proliferation, while they provide mechanical support, until the new bone tissue is formed at the affected area (25).

In order to promote bone regeneration it is necessary that the developed scaffolds fulfill some requirements like:

Biocompatibility: the scaffold is considered biocompatible when implanted in the body, it does not cause any immune rejection by the patient (3).

Biodegradability: materials used for the production of scaffolds may be biodegradable so that the rate of new bone formation may be accompanied by degradation of the provisory template, whose main function is to support cells, while the new tissue is being produced (31).

Osteoconduction: as defined by Davies *et al*. osteoconduction describes to the ability of the graft promote the migration of osteogenic cells to the surface of the scaffolds through a fibrin clot. This property assumes a large importance because it promotes neovascularization, that is very important for bone regeneration, ensuring the restoration the blood supply and promoting bone regeneration (25, 32).

Osteoinduction: this property is characterized the ability that scaffolds have to attract stem or osteoprogenitor cells to the bone healing site, promoting their differentiation into bone-forming OB (25). Considering that OB play a key role in the bone remodeling, scaffolds must have good properties of osteoinduction.

Mechanical properties: scaffolds should have sufficient mechanical strength to withstand the forces to which bone is daily subjected.

Porosity: scaffolds must have a porous structure and open pores that allow cell migration and proliferation. In addition, interconnectivity is also important for diffusion of nutrients (30).

1.4.2. Cell-biomaterial surface interactions

To assure that correct bone tissue regeneration occurs it is essentially that cell adheres to biomaterial surface when it is implanted in the organism. The process of cell adhesion occurs in three stages: cell adsorption, attachment and spreading (33). The first phase is characterized by an immediately adhesion, in which cells are deposited on the material's surface without cell spreading. In a second stage, the cells are attached to the material. Finally, in the last phase, cell spreading occurs, occurring changes in morphology resulting in cytoskeleton changes, thus creating a better interaction with the substrate (34, 35).
This interaction between cells and materials depends essentially on materials surface properties, such as their topography, hydrophilicity and chemical composition (36).

Topography: the roughness of material surface has effect on the osteoblastic cell attachment, proliferation and differentiation (37). Several studies have reported that materials with rough surfaces at micro and submicro scale with sizes similar to cells enhance osteoblast differentiation. On the other hand, materials with surfaces with higher roughness reduce cell adhesion due to the decreased surface area. Materials with low surface area decrease the ability of cells to establish contact area with the material (37).

Hydrophilicity: when a material is introduced into the body, water molecules are the first to reach to surface, thus the degree of hydrophilicity of the materials affects cell adhesion. This parameter is related to the contact angle/wettability of the materials that is defined as the ability of a liquid to be spread on a surface. The smaller the angle formed between the droplet and the substrate, the more hydrophilic will be surface and subsequently have a better cell adhesion (38).

Chemical composition: another parameter that affects the behavior of cells is the chemical composition of the material. Materials containing on its surface calcium and phosphate ions improve cell growth (39).

1.4.3. Materials used for scaffolds production

Metals, polymers and ceramics have been the most commonly used materials for the development of scaffolds for application in TE (25).
Metals are used in the development of bone substitutes due to mechanical properties that they present. Nevertheless, metals implants start to fail 10-15 years after being implanted in the body, being necessary its replacement frequently (25).

As alternative, biodegradable polymers of natural or synthetic origin has been used in TE. Synthetic polymers as poly (lactic acid) (PLA), Poly (glycolic acid) (PGA), poly (£-caprolactone) (PCL) are being applied in the field of biomedical engineering due to their good mechanical properties and also by the possibility of controlling the rate of degradation. However, they present some disadvantages, such as hydrophobic surfaces and poor cell adhesion, leading to the preferential use of natural polymers (25). These natural polymers include polysaccharides (starch, alginate, chitosan) or proteins-based polymers (collagen, fibrin gels, silk, and gelatin). Despite they present low mechanical strength, this natural polymers have high hydrophilicity, low immune reaction, as well as enhanced cell adhesion and proliferation (40).

Among these, Chitosan (CH) has gained quite popularity due to its intrinsic properties. CH is a cationic polysaccharide composed of copolymers of ß (1→4)-glucosamine and N-acetyl-D-glucosamine. This polymer of natural origin, derived from the deacetylation of chitin, which is the second most abundant biopolymer found in the shells of marine crustaceans and cell walls of fungi (41). Chitin and CH structures are presented in Figure 5.

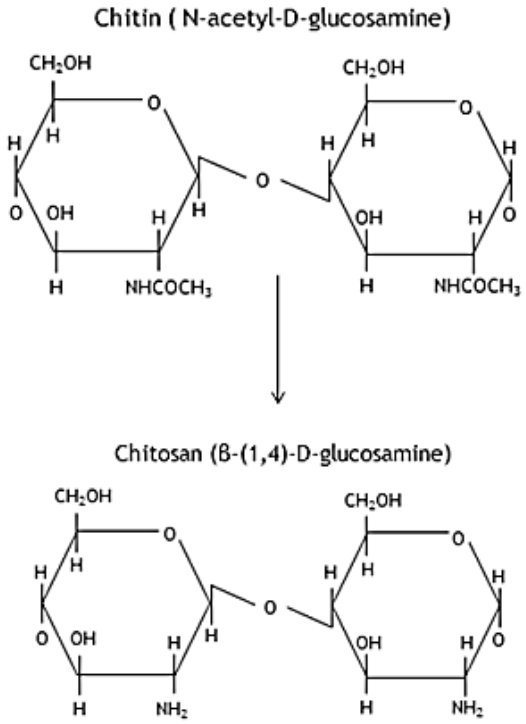

Figure 5: Chemical structure of chitin and chitosan (Adapted from (42, 43)).

CH is biocompatible, biodegradable, non-toxic and presents antibacterial properties (44, 45). Moreover, as mentioned above, due to its properties, CH has attracted much attention in the field of TE, being used for a wide variety of applications ranging from skin, bone and cartilage. Several studies have shown that CH has suitable properties for being used in scaffolds production that are aimed to be used in bone tissue engineering. Since it allows the production of structures with appropriate porosity and can support osteoblastic cell attachment, proliferation and differentiation, due to its hydrophilic character conferred by the presence hydroxyl and amine groups (46, 47). In spite of this, CH has some limitations like weak mechanical resistance and great instability, caused by its high capacity to swelling (48). Interestingly, several attempts have been made to enhance the intrinsic biological and mechanical properties of this polymer, through the incorporation of other natural polymers such as gelatin (GEL) (49).

GEL is a natural polymer derived from collagen, with valuable characteristics that allow their use in bone regeneration. It is biodegradable, biocompatible, has low antigenicity in comparison to collagen (50). Although, it being a precursors of collagen, it still retains some of the information signals, such as Arginine-Glycine-Asparagine (RGD) sequence, that promote cell adhesion, differentiation and proliferation (51).

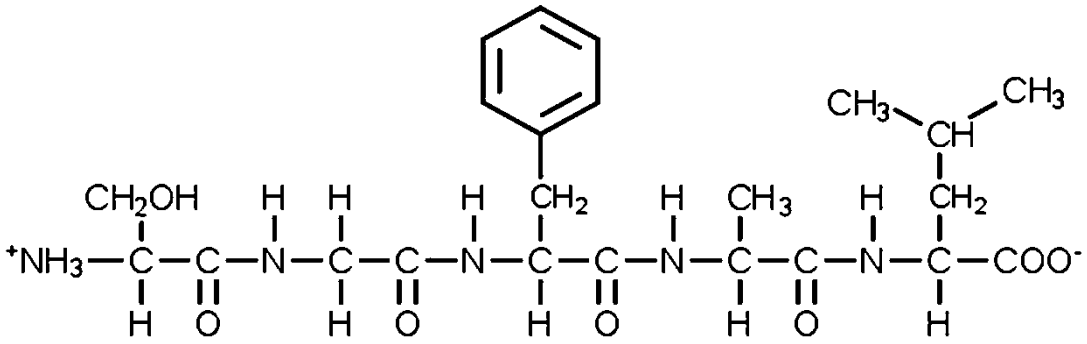

Figure 6: Chemical structure of gelatin (Adapted from (52)).

Although, both CH and GEL exhibit valuable properties to be used for bone regeneration, they still present weak mechanical resistance. Aiming to overcome this limitation, these natural polymers have been added to ceramics, such as hydroxyapatite (HA) and Beta Tricalcium Phosphate (ß-TCP). HA is the major inorganic component of bone and due its properties it has been used in production of scaffolds to be applied in bone tissue engineering. However, HA has some drawbacks. This ceramic presents low biodegradability and high costs. Conversely, Beta Tricalcium Phosphate (ß-TCP) present low cost and a higher degradation rate than HA. Moreover, ß-TCP is characterized by exhibiting a good bioactivity, biocompatibility, biodegradability and osteoconductivity (53).

1.4.4. Processing Techniques

Various methods have been explored in the development of scaffolds for bone tissue engineering, including solvent casting/particulate leaching, high pressure processing and freeze-drying.

As defined by Mikos *et al.* solvent casting/particulate leaching technique consists in a solution of a polymer dissolved in an organic solvent, with the incorporation of particles, mainly salts. This mixture is placed in a mold and subsequently freeze-dried in order to remove the solvent. The composite material obtained is thereafter placed in a bath to promote dissolution of the particles creating a porous structure (54). Although, this technique provides reasonable results for application in bone tissue engineering field, it presents some disadvantages. The use of organic solvents used may influence the cytotoxic profile of scaffolds (3).

The high pressure processing is other technique used in scaffolds production. This technique consists in the incorporation of gas bubbles at high pressure, usually carbone dioxide (CO2), in a polymer until saturation occurs. Through the decrease of pressure, the gas evaporates and creates macro-pores, resulting in a porous structure. Although this technique is not considered toxic, presents some disadvantages. The scaffolds produced have low mechanical properties, a non-porous surface and a closed pore structure, affecting this cell behavior (55).

Currently, it has been also used cryogenic processes, based on freezing-drying process (56). This technique is based on the freezing an aqueous solution followed by a process of sublimation through freeze-drying. The freeze-drying allows solvent remotion, under the action of vacuum and low pressure, resulting in a highly porous scaffolds (56). Conversely to solvent casting/particulate leaching technique, the freeze-drying uses non-toxic solvents, avoiding problems associated with toxicity. Furthemore and unlike the high pressure processing, this technique allows to produce highly porous structures with high pore interconnectivity (55).

1.5. Objectives

The main objective of this work was to develop scaffolds through freeze-drying for future application in bone tissue engineering. The present work plan had the following aims.

- In order to verify the effect of the incorporation gelatin and ß-TCP or both in CH scaffolds, various types of scaffolds (CH, CH/Gel, CH/ß-TCP and CH/Gel/ ß-TCP) were produced.

- Evaluation of the mechanical properties of the scaffolds.

- Evaluation and characterization of the biological properties of the scaffolds.

Chapter II

Materials and Methods

2.1. Materials

Amphotericin B, bovine serum albumin (BSA), dulbecco´s modified eagle´s medium (DMEM-F12), ethylenediaminetetraacetic acid (EDTA), glutaraldehyde, L-glutamine, medium molecular weight chitosan (MMW CH), penicillin G, phosphate buffered saline (PBS), sodium hydroxide (NaOH), sodium cacodylate, sodium tripolyphosphate (TPP), streptomycin, trypan blue and trypsin were purchased from Sigma-Aldrich (Sintra, Portugal). ßTCP was purchased from Pancreac (Barcelona, Spain). 3-(4,5-dimethylthiazol-2-yl)-5-(3-carboxymethoxyphenyl)-2-(4-sulfophenyl)-2H-tetrazolium reagent, inner salt (MTS) and electron coupling reagent (phenazine methosulfate; PMS) were acquired from Promega. Aqueous acetic acid was obtained from Pronalab. Fetal bovine serum (FBS) was purchased from Biochrom AG (Berlin, Germany). Human osteoblast cells (CRL-11372) were acquired to American Type Culture Collection (VA, USA).

2.2. Methods

2.2.1. Production of 3D Scaffolds

CH/GEL/ß-TCP 3D scaffolds were produced using the freeze-drying technique. Importantly, four different types of scaffolds were produced and tested, concerning their composition and the ratio used of different components (Table 3).

Table 3: Composition and ratios of different scaffolds produced in this study.

Scaffold	Constituents			Ratio
	Chitosan (CH)	Gelatin (Gel)	ß-TCP	% (wt)
Group I	X			
Group II	X	X		1:1
Group III	X		X	1:1
Group IV	X	X	X	2:1:1

To produce the four different formulations, CH 2% (w/v) was dissolved in a 1% aqueous acetic acid solution and maintained under magnetic stirring overnight, protected from light. Following, CH hydrogel preparation, the different types of scaffolds were produced. Briefly, scaffolds from Group I consisted only on CH hydrogel and those from Groups II and III were composed by a 1:1 ratio (% w/t) of CH hydrogel and Gelatin (Gel) and CH hydrogel and β-TCP,

respectively. Scaffolds from Group IV were produced after dispersion of Gel and β-TCP within the CH hydrogel (Table 3). In order to obtain homogenized hydrogels, all the mixtures were maintained under magnetic stirring, for 24 hours, sonicated and degassed in an ultrasound bath, for 10 minutes. Following this, all the solutions were deposited into a 48-well polystyrene plate, frozen for 24 hours at -20ºC and then lyophilized for 24 hours. The lyophilized 3D structures were removed from the molds and neutralized for 3 hours in a 1M NaOH (pH=12,8) solution. Then, the structures were washed for 10 minutes with Mili-Q ultrapure water and crosslinked with a 2,5% (w/v) (TPP) (pH=5,5) solution for 3 hours. Subsequently, they were washed again for 10 minutes. To conclude the production of the scaffolds, another similar cycle of freezing and freeze-dried was performed and the final 3D formulations were obtained.

2.2.2. Morphological characterization of the 3D scaffolds

2.2.2.1. Scanning Electron Microscopy (SEM) analysis

In order to evaluate the cellular behavior in the presence of the scaffolds, as well as the morphology and the diameter of the pores, Scanning Electron Microscopy (SEM) analysis was performed following the method adapted from Lima *et al.*(57). Accordingly, to prepare the 3D structures to be visualized by SEM, samples were washed twice with Phosphate Buffer Solution (PBS, pH=7.4), its fixed with 2.5 % (v/v) glutaraldehyde and then diluted in a 0.1 M sodium cacodylate solution. After 30 minutes in glutaraldehyde, the samples were washed twice with PBS and further dehydrated by incubation for 10 minutes in a graded series of ethanol solutions (50, 60, 70, 80, 90 and 99 % v/v). Next, samples were dried using CO_2 at critical point and finally sputtered-coated with gold using an Emitech K550 sputter coater (London, UK). SEM images were acquired with a Hitachi S-2700 (Tokyo, Japan) scanning electron microscope operating of 20 Kv at different amplifications.

2.2.3. Chemical and physical characterization of the scaffolds

2.2.3.1. Fourier Transform Infrared Spectroscopy Analysis

To evaluate the physicochemical characteristics of the manufactured 3D scaffolds Fourier Transform Infrared Spectroscopy (FTIR) analysis was performed. All the measurements were done using a Nicolet iS10 interferometer (Thermo Scientific, Waltham, MA, USA). Briefly, all the scaffolds were mounted on a diamond window and compressed to improve spectrum signal to noise ratio. For each sample, 128 interferograms were acquired with a spectral width ranging from 4000 to 500 cm^{-1} and a spectral resolution of 4 cm^{-1}. The acquired data was then processed in Omnic Spectra analysis software. CH, GEL and β-TCP alone were also analyzed to be used as control (58).

2.2.3.2. X-Ray Diffraction

To evaluate the crystalline phases and crystal orientation of the 3D scaffolds from the different groups, powder X-ray diffractometer (XRD) measurements were performed. CH, GEL and β-TCP samples were also analyzed to be used as a control. In order to perform to the XRD analysis of the materials, the samples were mounted in silica support using a double side adhesive tape. The data was recorded over a range of 5 ° to 90 ° 2θ degrees, with continuous scans at a rate of 1º/min, using a Rigaku Geigger Flex D-max III/C diffractometer with a copper ray tube operated at 30 kV and 20 mA (58).

2.2.3.3. Energy Dispersive Spectroscopy

In order to do an elemental characterization of scaffolds, Energy dispersive spectroscopy analysis (EDS) (Rontec) was also performed. Prior to perform all data acquisition, scaffolds were cut into slices and mounted in aluminum stub supports, air-dried at room temperature (RT) and sputter-coated with gold (59).

2.2.4. Mechanical characterization of the 3D scaffolds:

To characterize the mechanical properties of the four different scaffolds, four replicates of each sample were cut with a cylinder-shape and their respective dimensions measured. After that, the load at the time of the fracture and the strain that each sample can bear was obtained using a wick® 1435 Material prüfung (Ulm, Germany) with a crosshead speed of 0.2 mm/min and a load cell of 5 kN. Afterwards, compressive strength (Cs) of each type of scaffold was calculated by applying equation 1 (60).

$$Cs = \frac{F}{A} \qquad (1)$$

Where F is the load at the time of the fracture and A represent area of the scaffold.

2.2.5. Swelling Studies

The swelling capacity of scaffolds was determined by following a method adapted from Coimbra *et al*.(61). Scaffolds of the different groups were placed in eppendorfs containing 1ml of Tris buffer (pH=7, 4), at 37ºC. At predetermined intervals, the swollen samples were removed from the solution, the excess of Tris removed with filter paper, and samples were weighted. After weighed, the samples were reimmersed into the swelling medium.

The scaffolds were measured triplicate to get an average. The swelling ratio was evaluated by using equation 2:

$$\textbf{Swelling ratio (\%)} = \frac{Wt-W0}{W0} \times 100\% \qquad (2)$$

Where W_t is the final weight of scaffolds and $W_{0\,is}$ the initial weight of scaffolds.

2.2.5. Porosity Evaluation

The total porosity (P) of the different scaffolds was determined by liquid displacement method, using ethanol (EtOH), adapted from Nie *et al.*(62). In order to determine the total amount of ethanol absorbed by scaffolds, these were placed during 48 hours in absolute ethanol, and calculated by the following equation 3, adapted from Correia *et al.*(63) .

$$\mathbf{P}\ (\%) = \frac{\mathrm{W2} - \mathrm{W1}}{\mathrm{dethanol\ x\ Vscaffold}}\ \mathrm{x}\ 100 \qquad (3)$$

Where W2 and W1 represent wet and dry weight of the scaffolds, respectively, dethanol represents the density of the ethanol at room temperature and Vscaffold is the volume of the wet scaffold.

2.2.7. Biological characterization of the 3D Scaffolds

2.2.7.1. Culture of Osteoblasts in the presence of the scaffolds

Human osteoblasts cells (CRL-11372) were seeded at the surface of the structures. CRL-11372 cells were cultured in (DMEM-F12), supplemented with 10% heat inactivated FBS, streptomycin (100 µg /mL) and gentamicin (100 µg /mL), in 25 cm^2 T-flasks and maintained in a humidified atmosphere with 5% CO_2 at 37ªC. After cells reached confluence, they were detached using 0.18 % trypsin (1:250) and 5 mM EDTA Subsequently, cells were centrifuged during 5 minutes at 1300 rpm and then ressuspended in 5ml DMEM-F12. For distinguish between live and dead cells, they were counted in a Neubauer Chamber using trypan blue. In order to evaluate cell behavior in the presence of the scaffolds herein produced, cells were seeded on the scaffolds at a density $8.0x10^3$ cells/scaffold in 96-well Tissue Culture Polystyrene (TCPS) plates. Prior to cells seeding, scaffolds were sterilized during 30 minutes with ultraviolet radiation. Subsequently, they were placed in ethanol (EtOH) during 30 minutes and washed with PBS. Cell growth was monitored using an Olympus CX41 inverted light microscope (Tokyo, Japan) equipped with an Olympus SP-500 UZ digital camera.

2.2.7.2. Cytotoxic profile of scaffolds: MTS assay

In order to evaluate cytotoxic profile of the scaffolds, the MTS assay was performed, using method adapted from Ribeiro *et al.* All scaffolds herein produced were applied into a 96 well plate (n=5) and irradiated under UV light for 30 minutes before cell seeding. To perform the MTS assay cells were seeded in a 96 well plate containing the biomaterials, at a density of $10.0x10^3$ cells per well. Then, 100 µl of culture medium was added to each well and the plate was incubated at 37ºC, in a 5% CO_2 humified atmosphere.

After an incubation of 24, 48 and 72 h, the mitochondrial redox activity of the viable cells was assessed through the reduction of the MTS into a water-soluble purple formazan product.

At the indicated time points of culture, the medium of wells were removed and 100 µl medium was added to the wells with 20µl of MTS+PMS (phenazine methosulfate) reagent solution. The cells were incubated during 4 hours in a humidified atmosphere, at 37 ºC, with 5 % CO_2. Afterwards, 80 µL of the supernatant was transferred into a 96-well microplate and absorbance was measured at 492 nm using a microplate reader (Sanofi, Diagnostics Pauster). Wells containing cells in the culture medium without materials were used as negative control (K^-). Ethanol 96% was added to wells containing cells as a positive control (K^+).

2.2.6. Statistical analysis

The obtained results were expressed as the mean ± the standard error of the mean. The comparison of the various results obtained for different types of scaffolds was performed by using one-way analysis of variance (ANOVA), with the Dunnet´s post hoc test and Newman-Keuls test. A p value less than 0.05 ($p<0.05$) was deemed statistically significant.

Chapter III

Results and Discussion

3. Results and Discussion

3.1. Morphology and Macroscopic Properties of Scaffolds

As previously described, scaffolds developed for bone tissue regeneration must present adequate external and internal structures, as well as desirable physicochemical characteristics that mimic the ECM of bone and also adequate mechanical properties suitable to support the forces that bone is subject daily.

In this study, scaffolds was developed and optimized for being used in bone tissue regeneration. To achieve this goal, scaffolds were produced with natural polymers, namely CH and GEL, and ceramic, ß-TCP.

CH was chosen due to their intrinsic properties, namely biocompatibility, the ability to produce structures with appropriate porosity and able support osteoblastic cell attachment and proliferation (46, 64). The GEL was used due their biocompatibility and in order to improve properties of CH scaffolds (49, 50). Finally, ceramic ß-TCP was chosen based on its biocompatibility, biodegradability, osteoconductivity and the ability to increase the mechanical properties of scaffolds (65, 66).

Macroscopic images were acquired in order to characterize morphologic properties of the produced scaffolds. By analysis Figure 7, it is possible observe that despite using the same manufacturing process for all scaffolds, the images obtained revealed some differences between scaffolds. Observing the macroscopic images is possible conclude that CH scaffolds (Figure 7, image A) are those which present a less well-defined structure than other produced scaffolds. This is due to the fact that CH presents great instability and it is unable to maintain a predefined shape, as a result of its high capacity swelling (48). However, when adding mainly ß-TCP the production of scaffolds was observed that these present more well-defined structure than CH scaffolds (Figure 7, images C, D).

Moreover, it is possible observe that produced scaffolds present a porous structure, important to ensure bone regeneration. However, CH and CH/GEL scaffolds (Figure 7, images A, B) present a more porous structure than CH/ß-TCP and CH/GEL/ ß-TCP scaffolds (Figure 7, images C e B). This fact is due presence of ß-TCP that decrease the porosity of scaffolds, because the presence of hydroxyl groups belonging to ß-TCP and CH promote strong interaction between composite components (47, 67).

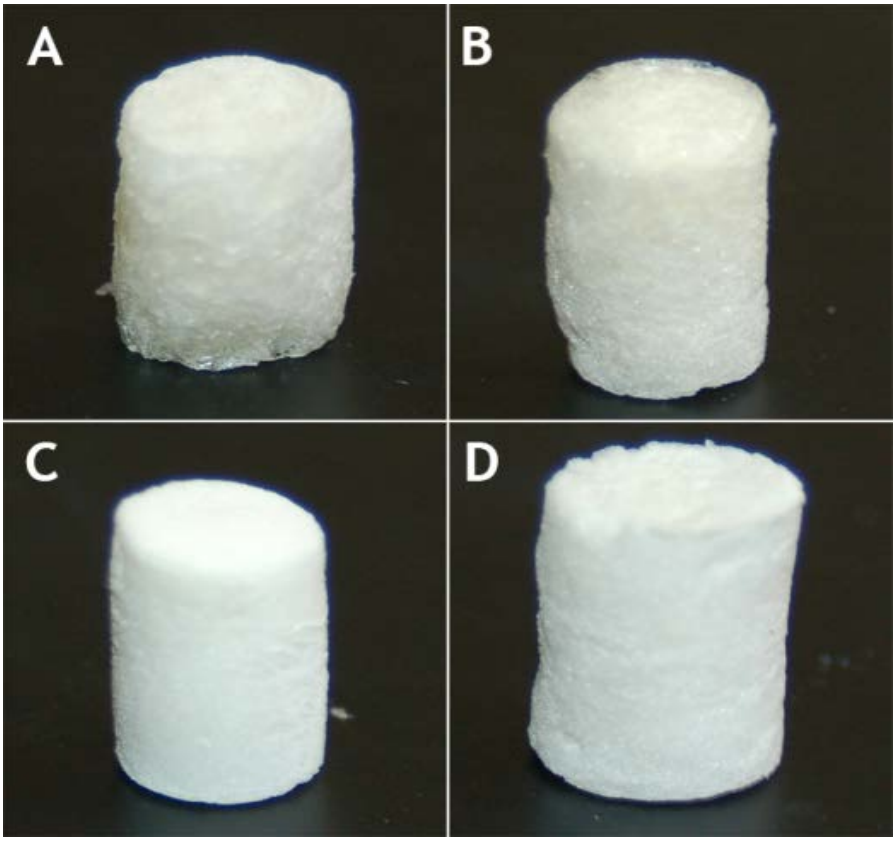

Figure 7: Macroscopic images of the different CH (A), CH/GEL (B), CH/ß-TCP (C) and CH/GEL/ß-TCP (D) scaffolds surface.

Afterwards, in order to characterize the morphology of scaffolds, namely surface features and pore sizes, SEM analysis was performed. By analyzing Figure 8, it is possible verify that scaffolds developed present porous and an interconnected structure. As previously described in literature, to ensure bone tissue regeneration it is necessary that scaffolds present porous structure and that porous be interconnected, allowing cell migration and proliferation, and nutrient flow (68).

Moreover, it is also possible to observed polymeric scaffolds have a smooth structure without irregularities, presenting a homogeneous structure (Figure 8, images A, B). However, when ß-TCP was added to scaffolds, structure becomes heterogeneous, presenting some irregularities (Figure 8, images C, D). These irregularities are due to deposition calcium and phosphate ions from ß-TCP, which are deposited on the surface of the biomaterial, increasing roughness (39). According to the literature, surface properties as roughness of the biomaterial are important in the process of cellular adhesion. Various studies have demonstrated that roughness of the material surface at micro and submicro scale improve the osteoblastic cell attachment, due the increase of surface area (37, 69). However, surfaces with high roughness reduce surface are, it leading decrease the ability of cells to establish contact are with the material.

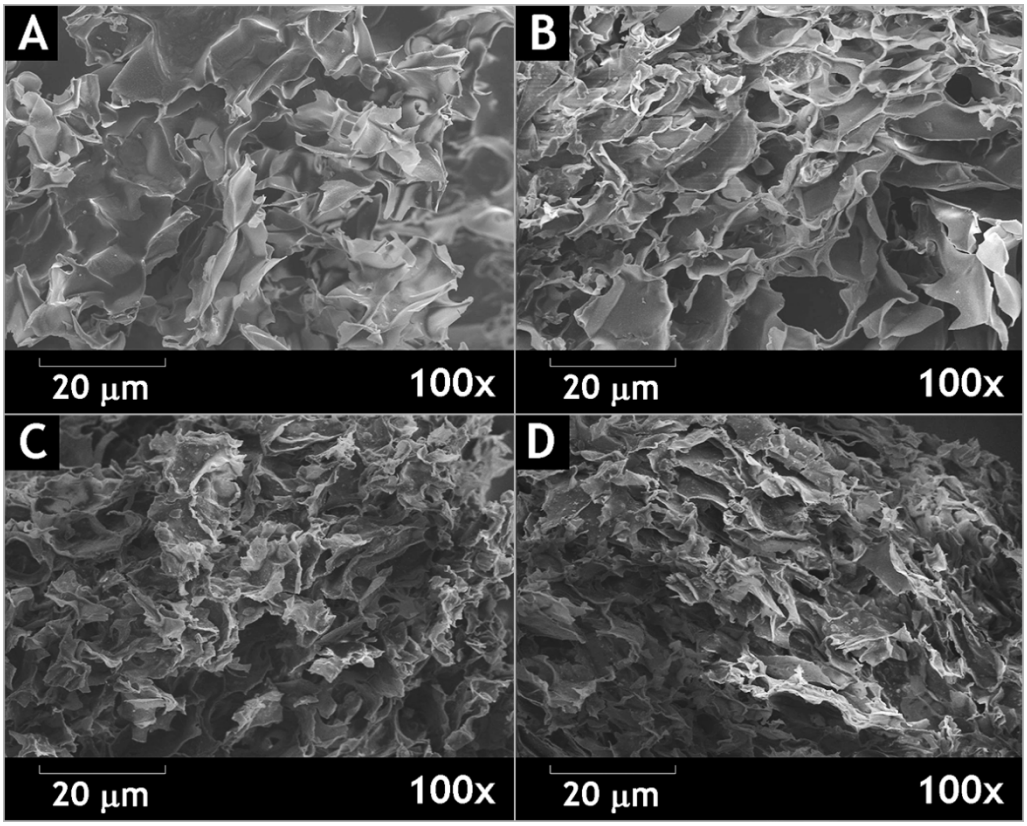

Figure 8: SEM images of the different scaffolds. Images show the surface characteristics of the CH (A), CH/GEL (B), CH/ß-TCP (C) and CH/GEL/ß-TCP (D) 3D scaffolds, respectively.

Mean pore size of the scaffolds was also determined by SEM analysis. CH and CH/GEL presented pores with values of 128 µm and 157 µm (Figure 9, images A, B), respectively, while CH/ ß-TCP and CH/GEL/ß-TCP presented values of 104 µm and 131 µm (Figure 9, images C, D). Based on the results obtained the scaffolds containing ß-TCP presented pores with a smaller diameter. As previously reported, pore size of scaffolds is another important condition for bone tissue regeneration. These should allow cell growth and migration and also nutrient diffusion. If pores are too small, cells will cover the pores, influencing cell migration and inhibiting neovascularization. On the other hand if these are too large reduce the surface are and subsequently cell adhesion. Although the optimal pore size for bone tissue engineering is not yet well-defined, recent studies have shown that pore with diameter values between 75-100 µm promote bone growth with an optimal range of 100-135µm. The scaffolds developed here present values pore size range of 104-157 µm (68). Thus, the results presented here in show that the scaffolds developed have a suitable pore size desirable to promote bone tissue regeneration.

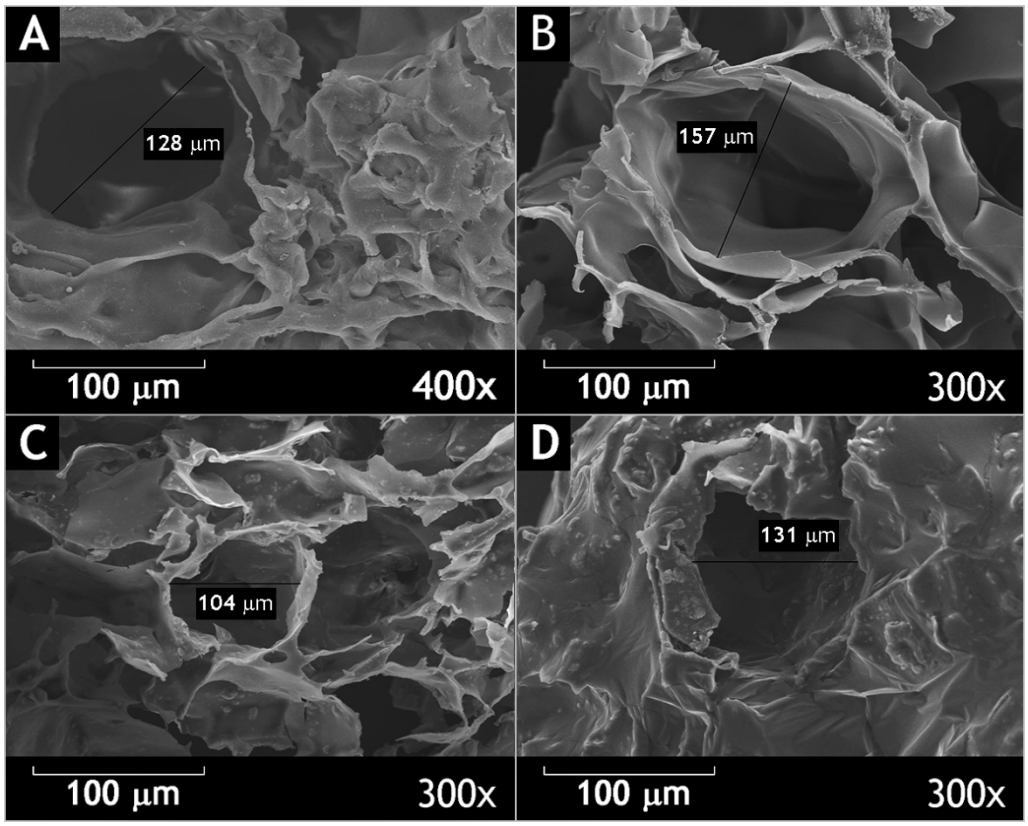

Figure 9: SEM images of pore size CH (A), CH/GEL (B), CH/ß-TCP (C) and CH/GEL/ß-TCP (D) scaffolds.

3.2. Physical-chemical characterization of the scaffolds

3.2.1. Fourier Transform Infrared Spectroscopy Analysis

To investigate the intermolecular interactions between the components of the scaffolds, ATR-FTIR analysis of CH, GEL and β-TCP alone and of the 3D scaffolds was carried out in the range of 500-4000 cm^{-1}. In Figure 10 it is possible to visualize FTIR spectra of CH, GEL and ß-TCP powder and CH, CH/GEL, CH/ ß-TCP and CH/GEL/ß-TCP scaffolds.

In previous studies it was reported the CH present characteristics peaks at 1657 cm^{-1} (C=O stretch in primary amide), 1603 cm^{-1} (NH2 deformation in primary amine), 1425 cm-1 (OH bending in carboxylic acids), 1319 cm^{-1} (amide III), 1084 cm^{-1}, 1033 cm^{-1} and 897 cm^{-1} (C-O) (70). GEL present bands at 3309 cm^{-1} (N-H in amines), 1653 cm^{-1} (C=O stretch in primary amide) and 1540 cm^{-1} (NH deformation in secondary amides (71, 72). ß -TCP presents a characteristics peak at 1061 cm^{-1} representative of P=O stretch in phosphates groups (70).

Besides, crosslink agent used, TPP present characteristic peaks at 890 and 1240 cm^{-1} correspondent polyions (P-OH and P=O stretches) (73).

FTIR spectra of CH powder (Figure 10) show peak around 1591 cm^{-1} that correspond amino groups. However, despite the peak also find in CH scaffolds, occurs a slight decrease. As described in the literature this slight decrease is due interaction that occurs between amine groups of CH and phosphate groups of TPP (73). In CH/GEL scaffolds is possible to visualize that besides the peaks corresponding to CH, there are also present characteristics bands of GEL. In addition, in the CH/ ß –TCP and CH/GEL/ß –TCP there is a new peak at around , characteristic of phosphate groups of ß –TCP, being more intense in scaffolds with higher amount ß –TCP (CH/ ß –TCP scaffolds).

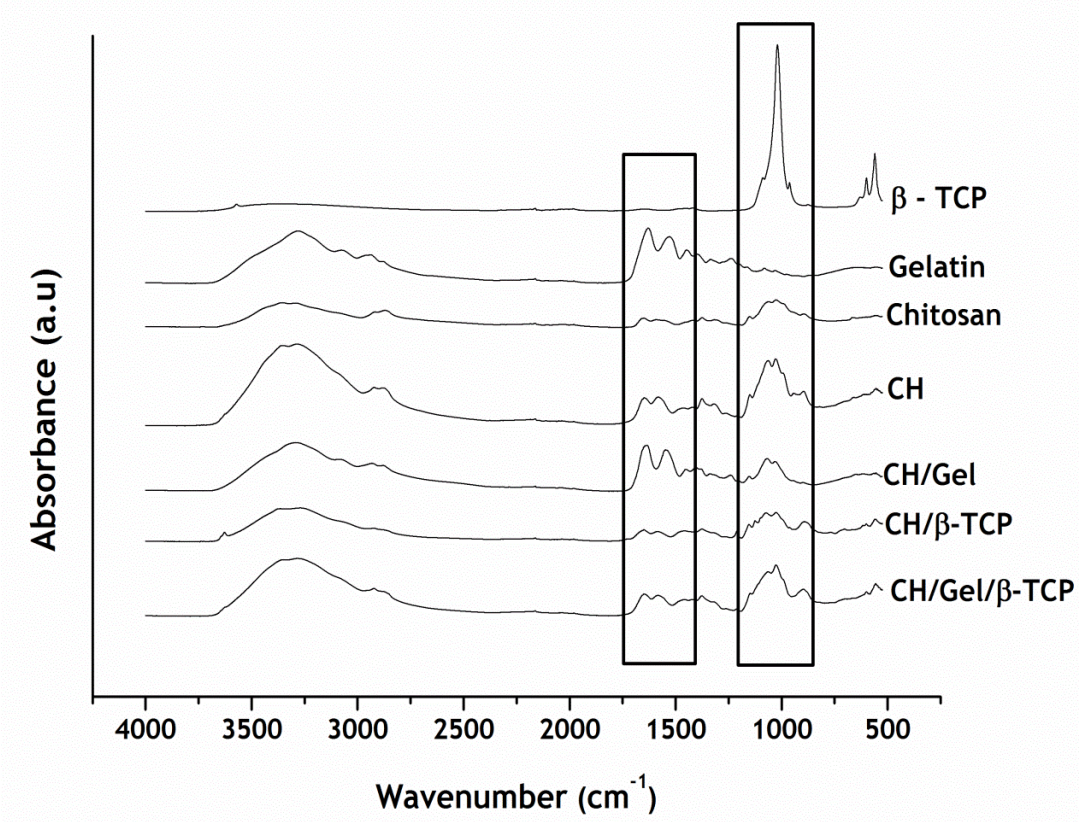

Figure 10: FTIR spectra for the CH, GEL and ß-TCP powder and different types of scaffolds.

3.2.2. X-Ray Diffraction analysis

XRD patterns of CH, GEL and ß-TCP powder and scaffolds are presented in Figure 11. As reported by Kim *et al.* CH presents a peak at 2Θ=19.6^{o} (67). By analysing Figure 11 it is possible to observe that a peak around 2Θ=20^{o} (*) was assigned to CH powder and CH scaffolds. Like CH the GEL spectra also shows a characteristic peak around at 2Θ=20º (**). CH/Gel scaffolds present peaks characteristics of polymers as it is possible observe through Figure 11. However, when ß-TCP is added for the production of scaffolds, this peak becomes wider and flatter. Furthermore, when this ceramic is introduced in the composition of scaffolds appears a new peak around 2Θ=33º (***) of ß-TCP, being these more intense in CH/ ß-TCP scaffolds, since it is the group that has higher amount of ß-TCP (58).

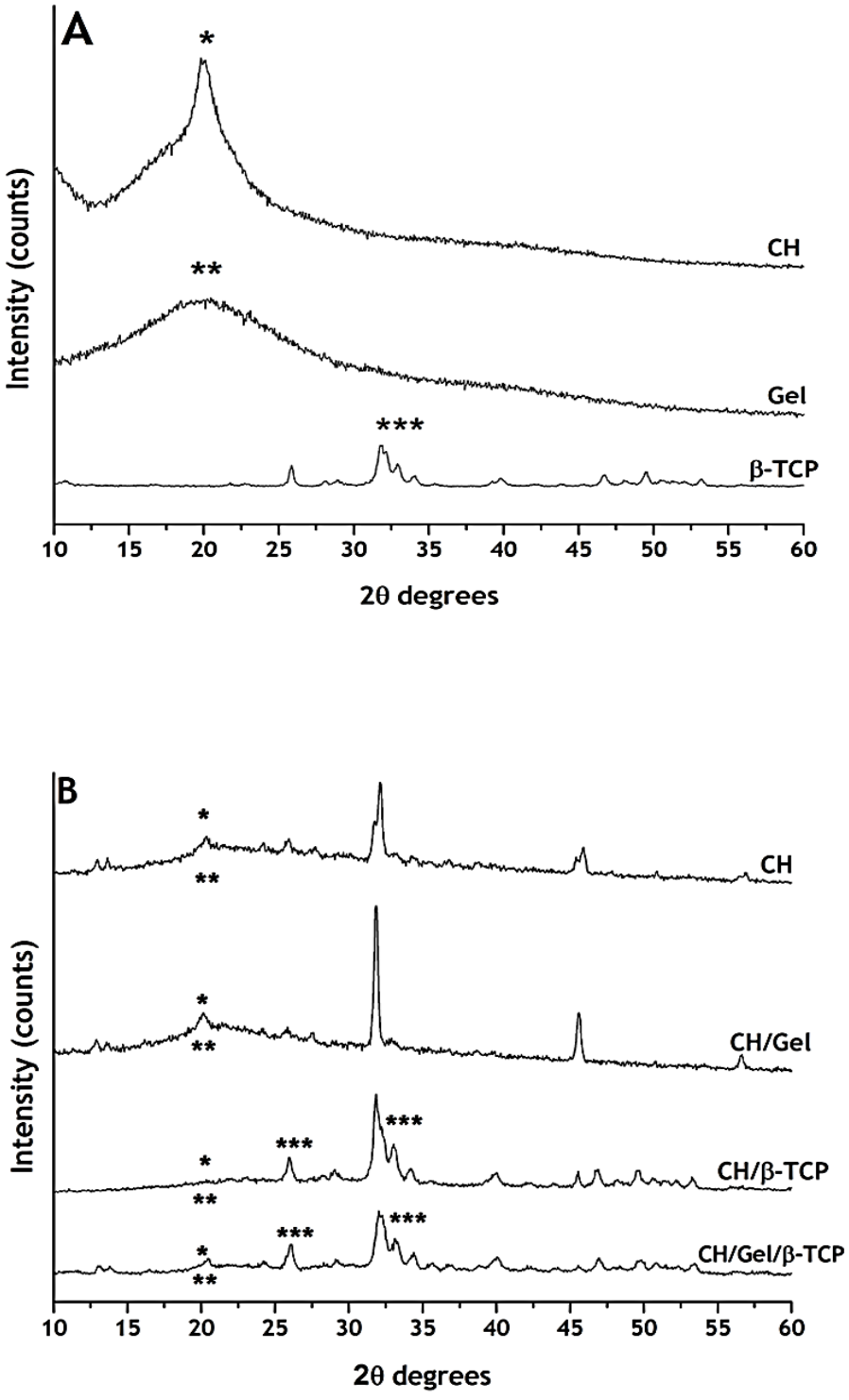

Figure 11: X-Ray spectra of a) pure CH, GEL and ß-TCP powders and b) groups I (CH), II (CH/GEL), III (CH/ß-TCP) and IV (CH/GEL/ ß-TCP) scaffolds (* characteristic peak of chitosan, ** characteristic peak o GEL and *** characteristic peak of ß-TCP).

3.2.4. Energy Dispersive Spectroscopy analysis

An Energy-Dispersive spectroscopy (EDS) analysis was also carried out with the purpose of characterize chemically the samples. The EDS results show the presence characteristic elements of the materials used for the production of scaffolds. From the analysis of the table 4 it turns out that all scaffolds present in their composition high amounts of carbon and oxygen elements. Considering that CH presents a chemical structure based on these elements and that it is present in their compositions of all scaffolds, the results obtained are in agreement. Moreover, also calcium and phosphate elements are present, and there is an increase in the CH/ß-TCP scaffolds, followed by CH/GEL/ß-TCP. These results are in agreement with the presence of ß-TCP in the composition of scaffolds. Finally, also sodium elements are present in the scaffolds. Although this element is not part of the constitution any of the materials used for the manufacture of scaffolds, its presence can be explained by the crosslinking agent used (TPP).

Table 2: Elemental analysis of the manufacture scaffolds

Sample	C	O	Na	P	Ca
CH	46.89	43.39	3.92	3.30	0.12
CH/GEL	45.53	46.52	3.50	3.14	-
CH/ß-TCP	43.72	43.84	2.45	8.15	9.56
CH/GEL/ß-TCP	29.88	43.95	5.82	4.59	4.35

3.3. Mechanical characterization of the 3D scaffolds

The mechanical properties, mainly resistance to compression of the material, are important data for the development of scaffolds to be applied in bone tissue regeneration. To evaluate the mechanical properties of scaffolds, compression strength was determined.

Through the analysis of Figure 12 it is possible to conclude that CH/ß-TCP, CH/GEL and CH/GEL/ß-TCP present greater compression strength when compared to CH scaffolds. In accordance to what is published in literature, the polymers used for the development scaffolds such as CH, alginate, presents weak mechanical properties, that limit their application in bone tissue engineering (74). Various studies have been performed for improving the mechanical resistance of scaffolds. Ceramics as hydroxyapatite (HA) and ß-TCP

have been studied for this purpose, because of its similarity to the inorganic phase of bone tissue. Thus, as has been described by Zhang composites of CH and calcium phosphate ceramics present better mechanical properties than CH scaffolds alone (75, 76). Besides, it is not only the incorporation of ceramics that increases resistance of scaffolds. Several studies have also shown that the CH blended with other polymers such as GEL, enhance the mechanical properties (49, 77). Thus, both GEL and ß-TCP have the ability enhance compressive strength of CH scaffolds. However, CH/ ß-TCP present better properties than CH/GEL scaffolds. For all this, it was expected that CHI/GEL/ ß-TCP scaffolds presented the better compressive strength, however this did not happened. One possible explanation for this is the fact that amount of ß-TCP was not enough to increase the compression strength of the scaffolds.

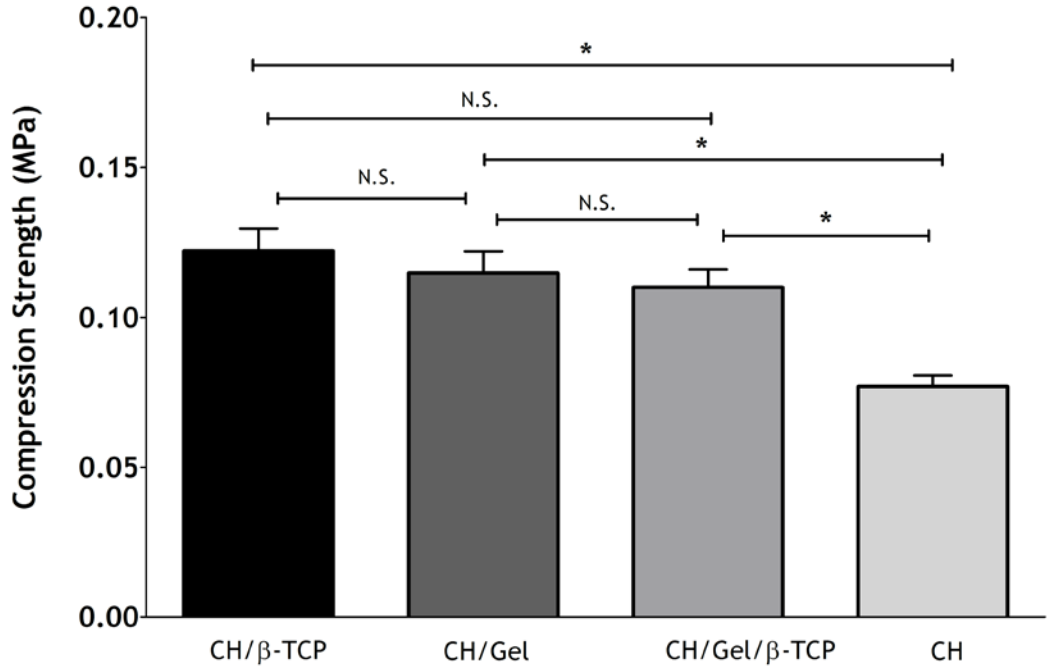

Figure 12: Characterization of the compressive strength of the scaffolds. Statistical analysis was performed using one-way ANOVA with Newman-Keuls tests (N.S.: not-significant, *p<0, 05).

3.4. Swelling Studies

Swelling and structural stability of scaffolds are also important factors that have to be characterized in the development of scaffolds for TE.
In order to evaluate the capacity of scaffolds produced herein have to absorb body fluids when introduced into organism, swelling studies were performed.

The swelling data of scaffolds is shown in Figure 13. All types of scaffolds exhibit a high capacity of swelling, which is indicative of their hydrophilic character. However, it was verified that CH and CH/GEL scaffolds present a higher swelling capacity than that of CH/ ß-TCP and CH/GEL/ ß-TCP scaffolds. According to the literature, CH and GEL confer the scaffolds hydrophilic nature and therefore a high swelling capacity. This property is due to the presence carboxyl, amine and hydroxyl groups in this structure (78, 79). However, the addition of HA or ß-TCP led to decrease the hydrophilic character and consequently a smaller swelling capacity of scaffolds. This is due to calcium and phosphorous groups of ß-TCP, that are bounded to groups that confer hydrophilicity of these polymers (78).

Moreover, through the analysis of Figure 13 it can be concluded that scaffolds presents maximum capacity swelling after 30 minutes, starting to stabilize immediately afterwards. This fact is important for TE because the initial swelling is important for promoting cell adhesion and growth, however swelling continuous leads to loss of mechanical integrity of scaffolds.

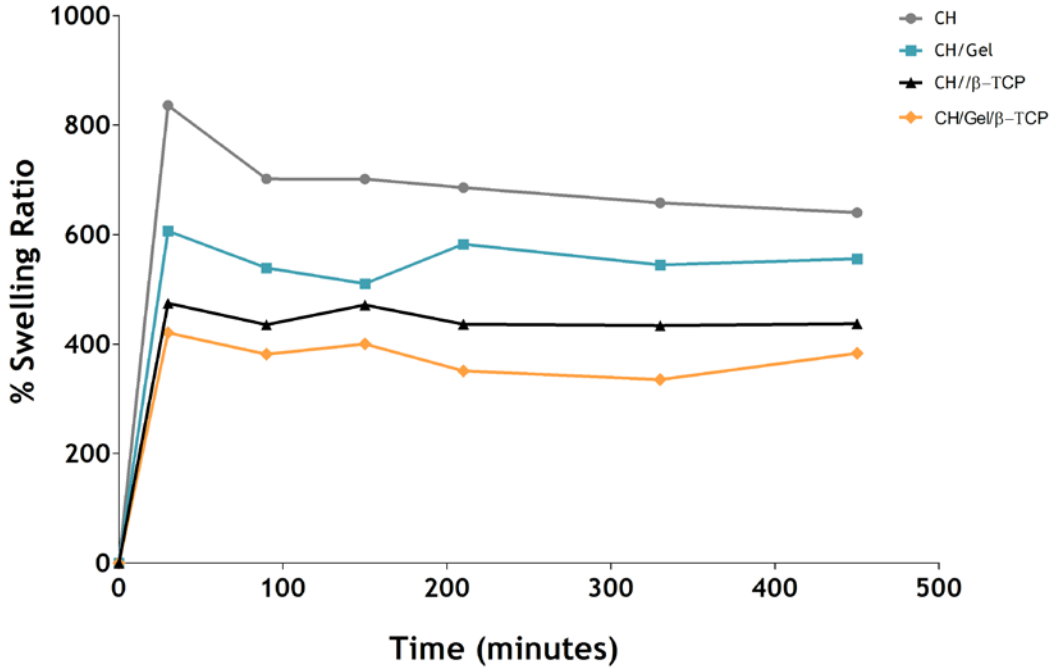

Figure 13: Swelling profile of the scaffolds.

3.5. Porosity

Scaffolds porosity was evaluated by using liquid displacement method, using ethanol. Figure 14 shows that all the scaffolds present porosity greater than 60%, a suitable value for bone regeneration (59). Moreover, the results obtained showed that the CH/Gel scaffolds present lower porosity than CH scaffolds. However, a statistically significant difference was observed only when ß-TCP was added scaffolds composition. Previous studies demonstrate that the presence of HA particles decrease the porosity (67). Thus, the statistically significant difference observed is due presence of ß-TCP that decrease porosity in CH/Gel/ß-TCP scaffolds and the lower polymer concentration in CH scaffolds, leading to increase of scaffolds porosity. As previously described, porosity of scaffolds is important to ensure bone regeneration. The porosity must be sufficient for allow cell growth and nutrient flow during bone regeneration, however, it also must have enough mechanical strength to support the frame during tissue regeneration.

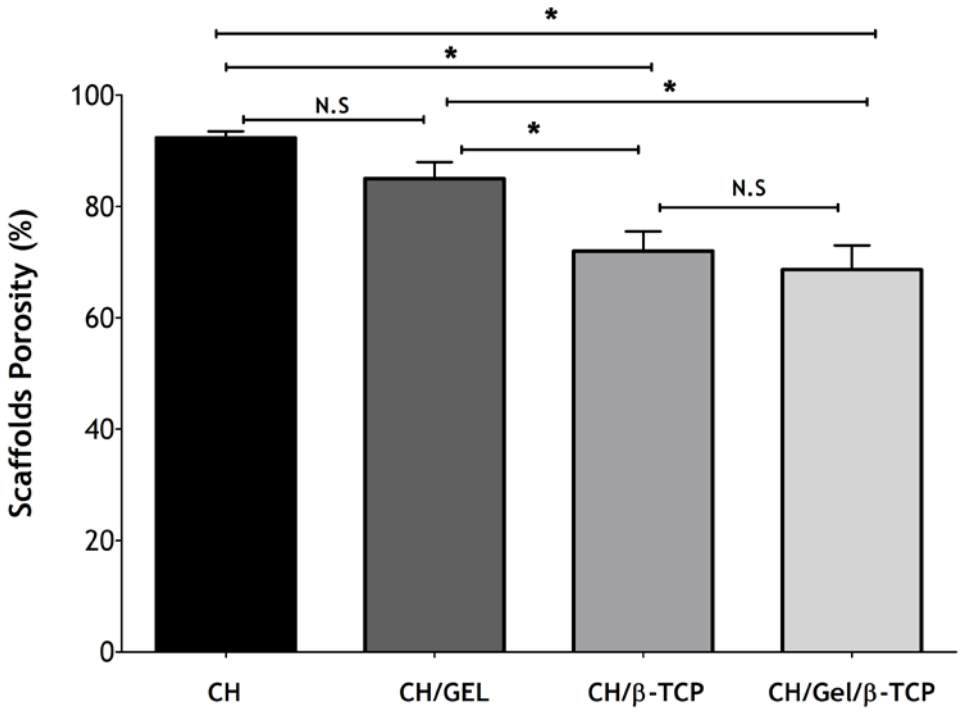

Figure 14: Total porosity of the different scaffolds. Statistical analysis was performed using one-way ANOVA with Newman-Keuls tests (N.S.: not-significant, *p<0, 05).

3.6. Analysis of the biological properties of the scaffolds

In vitro studies were performed to evaluate cytotoxic profile of the scaffolds. Human OB cells were seeded in the presence of scaffolds for up to 72 hours and their biocompatibility was evaluated at the indicated time points. Cell proliferation in the presence of the scaffolds was characterized by using an inverted light microscope (Figure 15).

The optical microscopy images acquired at 24, 48 and 72 hours after cell seeding showed the cells in contact with the scaffolds proliferated as well as in the negative control. However, in the positive control no cell proliferation was observed. Dead cells presented a typical spherical shape as can be observed in Figure 15.

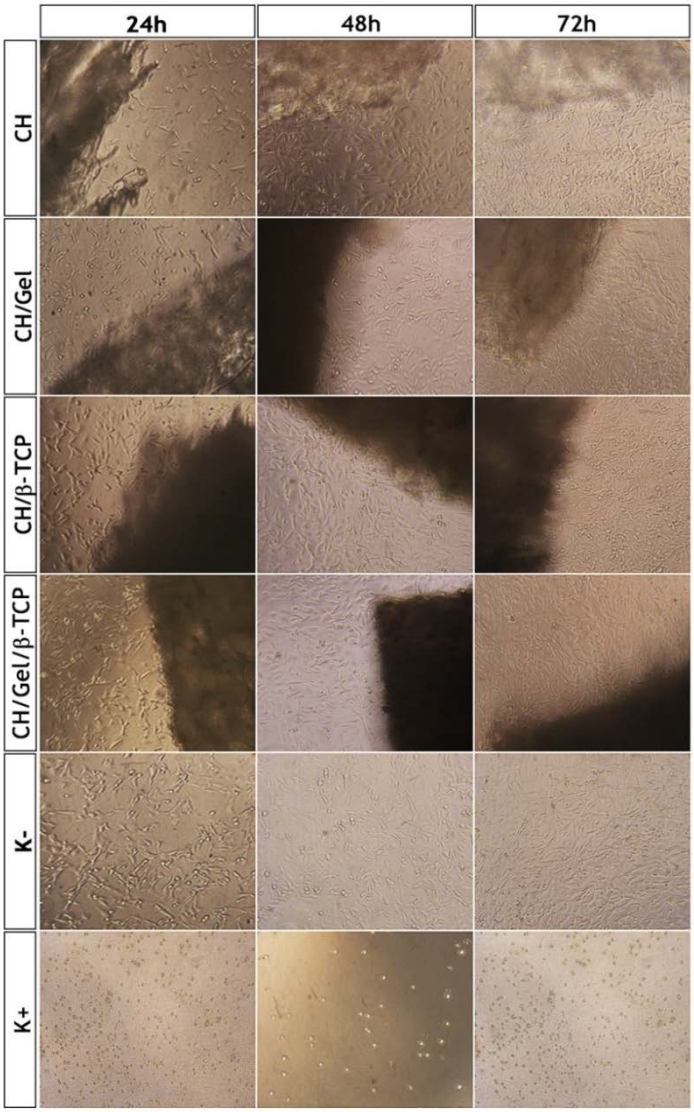

Figure 15: Microscopic images of human osteoblasts cells in the presence of scaffolds,during 24, 48 and 72 hours.

Moreover, the *in vitro* cytotoxic profile of the scaffolds was also characterized by an MTS assay. The results obtained (Figure 16) demonstrate that cells in contact with scaffolds present a higher cell viability than positive control, presenting statistically significant differences ($p<0,05$). It also showed a difference between the positive control and negative control ($p<0, 05$) and cells in contact with scaffolds. .

According to the literature, natural polymers, namely CH and GEL have been used in TE field due to its biocompatibility (49). Moreover, the incorporation of ceramics, like ß-TCP improve biological properties of CH scaffolds. The ß-TCP contains in its structure calcium and phosphate groups that are essential for the formation of new bone tissue.

Thus, the results obtained suggest that scaffolds developed have no acute cytotoxicity effect and cells proliferate on the scaffolds surface, which is fundamental for their application in bone tissue regeneration.

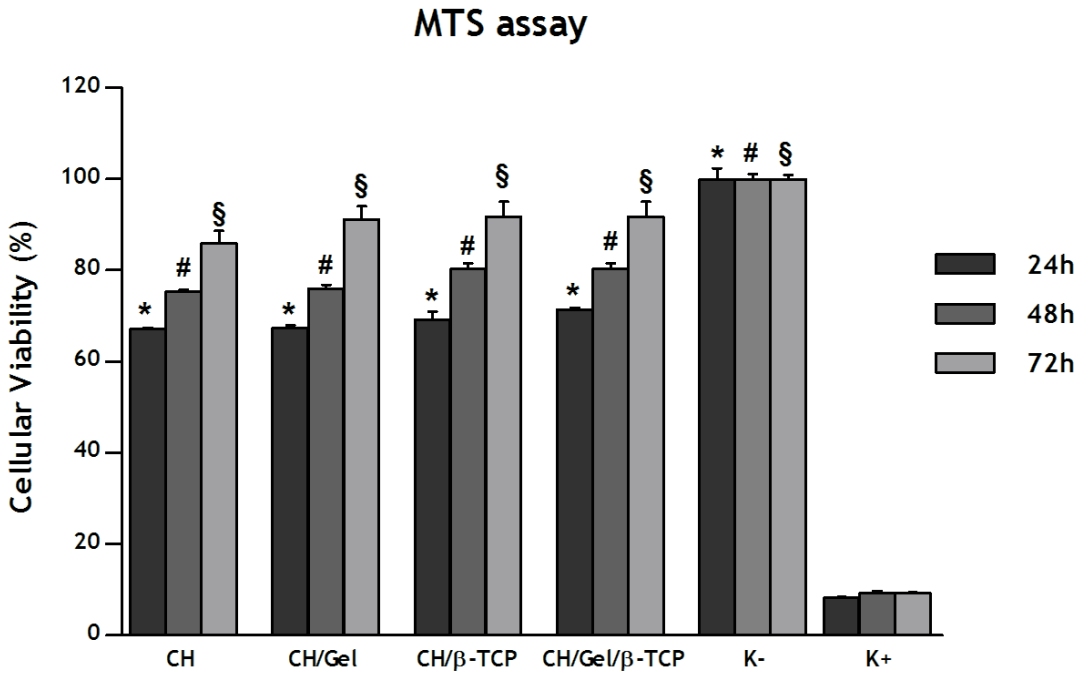

Figure 16: Evaluation of the cellular viability up to 72 hours by MTS assay. Negative control (K^-); Positive control (K^+), indicate viable and dead cells, respectively. Statistical analysis was performed using one-way ANOVA with Dunnet's post hoc test (*, #, § $p<0, 05$).

To confirm that human OB cells adhered to the surface of the materials a SEM analysis was also carried out. Figure 17 shows the SEM images of the cells in contact with different scaffolds produced after 24 and 72 hours. Through the analysis of the images obtained it is possible observe that in all types of scaffolds developed, the cells adhered and spread across scaffolds surface. After 72 hours the cells besides being adhered to the material, start to show the characteristic morphology of osteoblasts and acquired an extended configuration (filopodia).

Thus, is possible conclude that all types of scaffolds allow cell adhesion, namely human OB, essentially for promote bone regeneration.

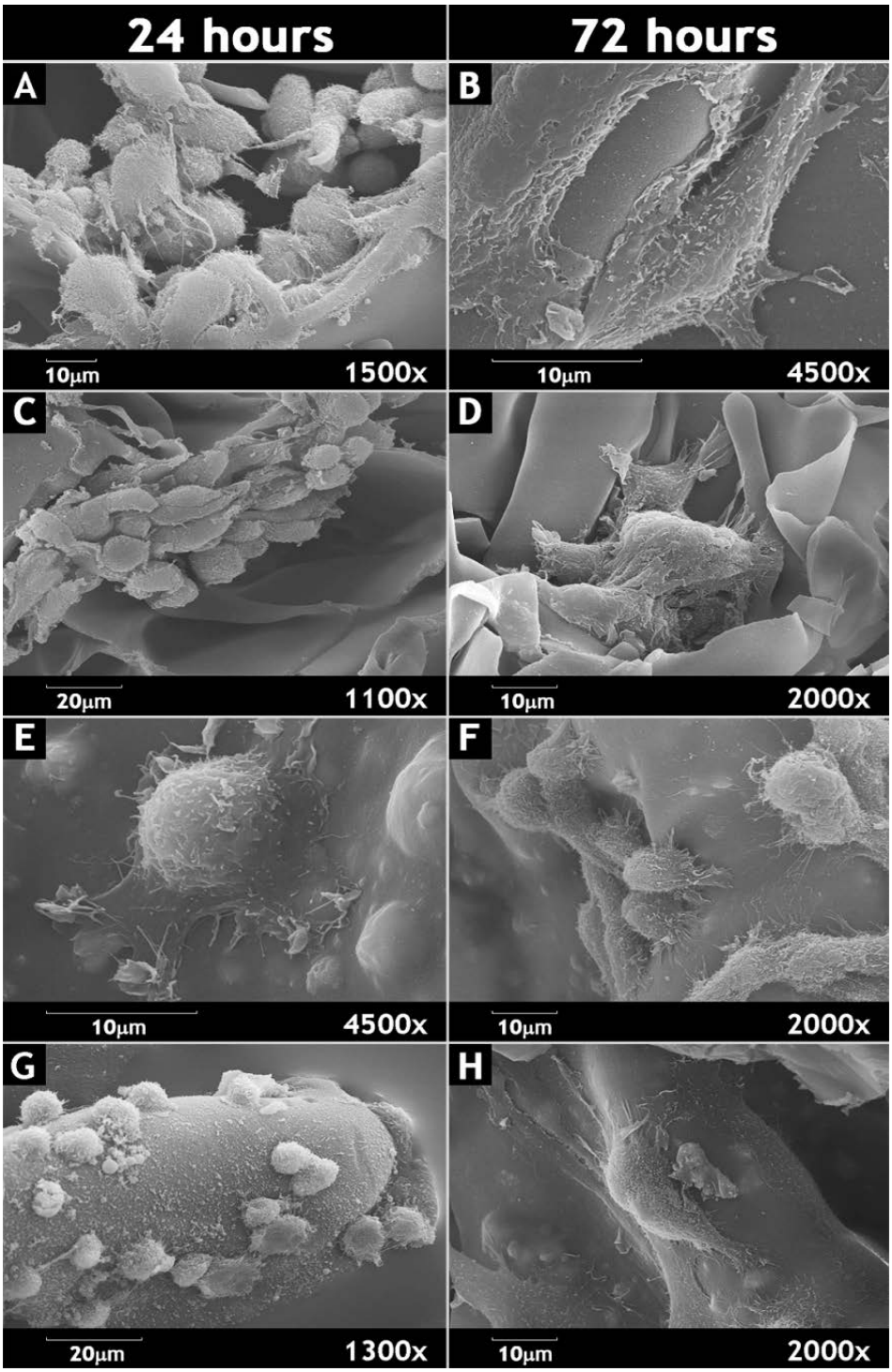

Figure 17: SEM micrographs of osteoblast morphology in the presence of the different scaffolds. SEM images were used to visualize osteoblast on the surface of the CH (A, B), CH/GEL (C,D), CH/ß-TCP (E,F) and CH/GEL/ß-TCP (G,H) 3D scaffolds, after being cultured for 24 hours (A,C,E and G) and 72 hours (B,D,F and H).

Chapter IV

Conclusion

4. Conclusion

In last years, millions of people worldwide have been suffering from bone defects due to trauma, tumors and bony diseases that, in some cases, may result in death. Several therapeutic approaches have been investigated in order to improve, restore or replace damaged tissue. Among the different bone substitutes developed so far, scaffolds are the most promising. These bone substitutes possess the essential properties that are required for bone regeneration and mimic the structure of ECM that provide a favorable microenvironment for cell adhesion and proliferation.

In the present study different scaffolds were produced using a freeze-dry technique in order to be used in a near future in bone tissue engineering. Four types of scaffolds were successfully produced herein: CH; CH/GEL; CH/ß-TCP and CH/GEL/ ß-TCP, in order to study the influence of the incorporation of gelatin and ß-TCP in structure of CH scaffolds.

In this study different assays were performed in order to characterize scaffolds structure through SEM, FTIR, XRD and EDS. SEM analysis of scaffolds showed a porous and interconnected structure, allowing cell migration and proliferation, as well as nutrient flow. Besides, SEM images showed that the incorporation of ß-TCP in scaffolds enhance their roughness, that is important for cell adhesion. The results of FTIR, XRD and EDS prove that the blend between of materials was achieved.

Moreover, the mechanical resistance of scaffolds was also evaluated. The results showed that incorporation of GEL and ß-TCP in CH scaffolds increased significantly the mechanical resistance of the scaffolds. However, the results obtained were lower than compression strength of trabecular and cortical bone.

Porosity and swelling behaviour of scaffolds were also evaluated. The results demonstrated that all types of scaffolds produced have porosity higher than 60%, a suitable value for bone regeneration. However, the incorporation of ß-TCP promoted a decrease in scaffolds porosity which is agreement with the results obtained in mechanical analysis. Regarding the swelling capacity, all types of scaffolds presented a similar swelling behaviour. However, the incorporation of ß-TCP impaired the swelling capacity of scaffolds.

Furthemore, SEM analysis of scaffolds showed that human osteoblasts adhered to material surface. Moreover, cell viability was also assessed by MTS assay and the results confirmed that human osteoblasts remain viable in contact with scaffolds. Based in the in vitro results the developed scaffolds promote cell adhesion and proliferation and do not exhibit cytotoxic effect for the cells, which is fundamental for their application in bone tissue regeneration.

In a near future, the mechanical properties will be improved once the values obtained are far of "ideal" values. To achieve this purpose several strategies must be applied. Firstly, increasing the concentration of CH solution and the viscosity of the final solution, subsequently, would increase the mechanical resistance of the scaffolds. Besides, the ratios between CH, Gel and β-TCP must be optimized. Another strategy would be replacing β-TCP by other ceramic more resistance, such as hydroxyapatite.

Chapter V
Bibliography

5. Bibliography

1. Van De Graaff KM. Human Anatomy. 6th ed: The McGraw-Hill Companies, Inc.; 2002.

2. Seeley RR, Stephens TD, Tate P. Anatomia & Fisiologia. 8th ed: Lusociência-Edições Técnicas e Científicas, Lda.; 2008.

3. Salgado AJ, Coutinho OP, Reis RL. Bone tissue engineering: state of the art and future trends. Macromolecular bioscience. 2004;4(8):743-65.

4. Marieb EN, Hoehn K. Human Anatomy & Physiology. 7th ed: Pearson Education, Inc.; 2007.

5. Murugan R, Ramakrishna S. Development of nanocomposites for bone grafting. Composites Science and Technology. 2005;65(15):2385-406.

6. Ralston SH. Structure and metabolism of bone. Medicine. 2005;33(12):58-60.

7. Mackie E. Osteoblasts: novel roles in orchestration of skeletal architecture. The international journal of biochemistry & cell biology. 2003;35(9):1301-5.

8. Jayakumar P, Di Silvio L. Osteoblasts in bone tissue engineering. Proceedings of the Institution of Mechanical Engineers, Part H: Journal of Engineering in Medicine. 2010;224(12):1415-40.

9. Torres A, Santos S, Oliveira M, Barbosa M. Fibrinogen promotes resorption of chitosan by human osteoclasts. Acta biomaterialia. 2013; 9 (5):6553-62.

10. Schindeler A, McDonald MM, Bokko P, Little DG, editors. Bone remodeling during fracture repair: the cellular picture. Seminars in cell & developmental biology; 2008; 19(5): 459-466.

11. Jang J-H, Castano O, Kim H-W. Electrospun materials as potential platforms for bone tissue engineering. Advanced Drug Delivery Reviews. 2009;61(12):1065-83.

12. Feng X, McDonald JM. Disorders of bone remodeling. Annual review of pathology. 2011;6:121.

13. Raggatt LJ, Partridge NC. Cellular and molecular mechanisms of bone remodeling. Journal of Biological Chemistry. 2010;285(33):25103-8.

14. Sims NA, Gooi JH, editors. Bone remodeling: Multiple cellular interactions required for coupling of bone formation and resorption. Seminars in cell & developmental biology; 2008; 19(5): 444-451.

15. Datta H, Ng W, Walker J, Tuck S, Varanasi S. The cell biology of bone metabolism. Journal of clinical pathology. 2008;61(5):577-87.

16. Boyce BF, Xing L. Functions of RANKL/RANK/OPG in bone modeling and remodeling. Archives of biochemistry and biophysics. 2008;473(2):139-46.

17. Väänänen HK, Laitala-Leinonen T. Osteoclast lineage and function. Archives of biochemistry and biophysics. 2008;473(2):132-8.

18. Robling AG, Castillo AB, Turner CH. Biomechanical and molecular regulation of bone remodeling. Annu Rev Biomed Eng. 2006;8:455-98.

19. Weitzmann MN, Pacifici R. Estrogen deficiency and bone loss: an inflammatory tale. Journal of Clinical Investigation. 2006;116(5):1186-94.

20. Djouad F, Guerit D, Marie M, Toupet K, Jorgensen C, Noel D. Mesenchymal Stem Cells: New Insights into Bone Regenerative Applications. Journal of Biomaterials and Tissue Engineering. 2012;2(1):14-28.

21. Peel N. Bone remodelling and disorders of bone metabolism. Surgery (Oxford). 2009;27(2):70-4.

22. Mazziotti G, Canalis E, Giustina A. Drug-induced osteoporosis: mechanisms and clinical implications. The American journal of medicine. 2010;123(10):877-84.

23. Ngiam M, Nguyen L, Liao S, Chan CK, Ramakrishna S. Biomimetic nanostructured materials: Potential regulators for osteogenesis. Ann Acad Med Singapore. 2011;40(5):213-22.

24. Murugan R, Ramakrishna S. Bioresorbable composite bone paste using polysaccharide based nano hydroxyapatite. Biomaterials. 2004;25(17):3829-35.

25. Chiara G, Letizia F, Lorenzo F, Edoardo S, Diego S, Stefano S, et al. Nanostructured biomaterials for tissue engineered bone tissue reconstruction. International journal of molecular sciences. 2012;13(1):737-57.

26. Van der Stok J, Van Lieshout EM, El-Massoudi Y, Van Kralingen GH, Patka P. Bone substitutes in the Netherlands–A systematic literature review. Acta biomaterialia. 2011;7(2):739-50.

27. Giannoudis PV, Dinopoulos H, Tsiridis E. Bone substitutes: an update. Injury. 2005;36(3):S20-S7.

28. Kneser U, Schaefer D, Polykandriotis E, Horch R. Tissue engineering of bone: the reconstructive surgeon's point of view. Journal of cellular and molecular medicine. 2006;10(1):7-19.

29. Robert L, Vacanti JP. Tissue engineering. Science. 1993;260(2):920-41.

30. Karageorgiou V, Kaplan D. Porosity of 3D biomaterial scaffolds and osteogenesis. Biomaterials. 2005 Sep;26(27):5474-91.

31. Ma PX. Biomimetic materials for tissue engineering. Advanced drug delivery reviews. 2008;60(2):184-98.

32. Davies J. Mechanisms of endosseous integration. The International journal of prosthodontics. 1997;11(5):391-401.

33. Anselme K. Osteoblast adhesion on biomaterials. Biomaterials. 2000;21(7):667-81.

34. Choi CK, Breckenridge MT, Chen CS. Engineered materials and the cellular microenvironment: a strengthening interface between cell biology and bioengineering. Trends in cell biology. 2010;20(12):705-14.

35. Lee JW, Kim YH, Park KD, Jee KS, Shin JW, Hahn SB. Importance of integrin< i> β</i> 1-mediated cell adhesion on biodegradable polymers under serum depletion in mesenchymal stem cells and chondrocytes. Biomaterials. 2004;25(10):1901-9.

36. Anselme K, Bigerelle M. Topography effects of pure titanium substrates on human osteoblast long-term adhesion. Acta Biomaterialia. 2005;1(2):211-22.

37. Gittens RA, McLachlan T, Olivares-Navarrete R, Cai Y, Berner S, Tannenbaum R, et al. The effects of combined micron-/submicron-scale surface roughness and nanoscale features on cell proliferation and differentiation. Biomaterials. 2011;32(13):3395-403.

38. Zhu X, Chen J, Scheideler L, Reichl R, Geis-Gerstorfer J. Effects of topography and composition of titanium surface oxides on osteoblast responses. Biomaterials. 2004;25(18):4087-103.

39. Zhu X, Kim K-H, Jeong Y. Anodic oxide films containing Ca and P of titanium biomaterial. Biomaterials. 2001;22(16):2199-206.

40. Swetha M, Sahithi K, Moorthi A, Srinivasan N, Ramasamy K, Selvamurugan N. Biocomposites containing natural polymers and hydroxyapatite for bone tissue engineering. International journal of biological macromolecules. 2010;47(1):1-4.

41. Di Martino A, Sittinger M, Risbud MV. Chitosan: a versatile biopolymer for orthopaedic tissue-engineering. Biomaterials. 2005;26(30):5983-90.

42. Shi C, Zhu Y, Ran X, Wang M, Su Y, Cheng T. Therapeutic potential of chitosan and its derivatives in regenerative medicine. Journal of Surgical research. 2006;133(2):185-92.

43. Thein-Han W, Kitiyanant Y, Misra R. Chitosan as scaffold matrix for tissue engineering. Materials Science and Technology. 2008;24(9):1062-75.

44. Jiang T, Deng M, James R, Nair LS, Laurencin CT. Micro-and nanofabrication of chitosan structures for regenerative engineering. Acta biomaterialia. 2013;

45. Li Y, Wang Y, Wu D, Zhang K, Hu Q. A facile approach to construct three-dimensional oriented chitosan scaffolds with in-situ precipitation method. Carbohydrate polymers. 2010;80(2):408-12.

46. Amaral I, Sampaio P, Barbosa M. Three-dimensional culture of human osteoblastic cells in chitosan sponges: The effect of the degree of acetylation. Journal of Biomedical Materials Research Part A. 2006;76(2):335-46.

47. Tanase C, Popa M, Verestiuc L. Biomimetic bone scaffolds based on chitosan and calcium phosphates. Materials Letters. 2011;65(11):1681-3.

48. Li Z, Ramay HR, Hauch KD, Xiao D, Zhang M. Chitosan–alginate hybrid scaffolds for bone tissue engineering. Biomaterials. 2005;26(18):3919-28.

49. Huang Y, Onyeri S, Siewe M, Moshfeghian A, Madihally SV. In vitro characterization of chitosan–gelatin scaffolds for tissue engineering. Biomaterials. 2005;26(36):7616-27.

50. Malafaya PB, Silva GA, Reis RL. Natural–origin polymers as carriers and scaffolds for biomolecules and cell delivery in tissue engineering applications. Advanced drug delivery reviews. 2007;59(4):207-33.

51. Lien S-M, Ko L-Y, Huang T-J. Effect of pore size on ECM secretion and cell growth in gelatin scaffold for articular cartilage tissue engineering. Acta biomaterialia. 2009;5(2):670-9.

52. Zhang D, Yang H. Gelatin-stabilized copper nanoparticles: Synthesis, morphology, and their surface-enhanced Raman scattering properties. Physica B: Condensed Matter. 2013; 415: 44-48.

53. Cao H, Kuboyama N. A biodegradable porous composite scaffold of PGA/β-TCP for bone tissue engineering. Bone. 2010;46(2):386-95.

54. Mikos AG, Thorsen AJ, Czerwonka LA, Bao Y, Langer R, Winslow DN, et al. Preparation and characterization of poly (L-lactic acid) foams. Polymer. 1994;35(5):1068-77.

55. Leong K, Cheah C, Chua C. Solid freeform fabrication of three-dimensional scaffolds for engineering replacement tissues and organs. Biomaterials. 2003;24(13):2363-78.

56. Fukasawa T, Deng Z-Y, Ando M, Ohji T, Goto Y. Pore structure of porous ceramics synthesized from water-based slurry by freeze-dry process. Journal of Materials Science. 2001;36(10):2523-7.

57. Lima AC, Batista P, Valente TA, Silva AS, Correia IJ, Mano JF. Novel Methodology Based on Biomimetic Superhydrophobic Substrates to Immobilize Cells and Proteins in Hydrogel Spheres for Applications in Bone Regeneration. Tissue Engineering Part A. 2013;19(9-10):1175-87.

58. Santos CFL, Silva AP, Lopes L, Pires I, Correia IJ. Design and production of sintered β-tricalcium phosphate 3D scaffolds for bone tissue regeneration. Materials Science and Engineering: C. 2012;32(5):1293-8.

59. Torres A, Gaspar V, Serra I, Diogo G, Fradique R, Silva A, et al. Bioactive Polymeric-Ceramic Hybrid 3D Scaffold for Application in Bone Tissue Regeneration. Materials Science and Engineering: C. 2013; 33(7): 4460-69.

60. Wu X, Liu Y, Li X, Wen P, Zhang Y, Long Y, et al. Preparation of aligned porous gelatin scaffolds by unidirectional freeze-drying method. Acta Biomaterialia. 2010 ;6(3):1167-77.

61. Coimbra P, Alves P, Valente T, Santos R, Correia I, Ferreira P. Sodium hyaluronate/chitosan polyelectrolyte complex scaffolds for dental pulp regeneration: synthesis and characterization. International journal of biological macromolecules. 2011;49(4):573-9.

62. Nie HL, Zhu LM. Adsorption of papain with Cibacron Blue F3GA carrying chitosan-coated nylon affinity membranes. International journal of biological macromolecules. 2007;40(3):261-7.

63. Correia TR, Antunes BP, Castilho PH, Nunes JC, Pessoa de Amorim MT, Escobar IC, et al. A bi-layer electrospun nanofiber membrane for plasmid DNA recovery from fermentation broths. Separation and Purification Technology. 2013; 112: 20-25.

64. Dash M, Chiellini F, Ottenbrite R, Chiellini E. Chitosan—A versatile semi-synthetic polymer in biomedical applications. Progress in Polymer Science. 2011;36(8):981-1014.

65. Yang Y, Bumgardner J, Cavin R, Carnes D, Ong J. Osteoblast precursor cell attachment on heat-treated calcium phosphate coatings. Journal of dental research. 2003;82(6):449-53.

66. Suzuki T, Yamamoto T, Toriyama M, Nishizawa K, Yokogawa Y, Mucalo MR, et al. Surface instability of calcium phosphate ceramics in tissue culture medium and the effect on adhesion and growth of anchorage-dependent animal cells. Journal of biomedical materials research. 1997;34(4):507-17.

67. Kim HS, Kim JT, Jung YJ, Ryu SC, Son HJ, Kim YG. Preparation of a porous chitosan/fibroin-hydroxyapatite composite matrix for tissue engineering. Macromolecular Research. 2007;15(1):65-73.

68. Murphy CM, Haugh MG, O'Brien FJ. The effect of mean pore size on cell attachment, proliferation and migration in collagen–glycosaminoglycan scaffolds for bone tissue engineering. Biomaterials. 2010;31(3):461-6.

69. Raines AL, Olivares-Navarrete R, Wieland M, Cochran DL, Schwartz Z, Boyan BD. Regulation of angiogenesis during osseointegration by titanium surface microstructure and energy. Biomaterials. 2010;31(18):4909-17.

70. Manjubala I, Scheler S, Bössert J, Jandt KD. Mineralisation of chitosan scaffolds with nano-apatite formation by double diffusion technique. Acta Biomaterialia. 2006;2(1):75-84.

71. Mi F-L. Synthesis and characterization of a novel chitosan-gelatin bioconjugate with fluorescence emission. Biomacromolecules. 2005;6(2):975-87.

72. Kim S, Nimni ME, Yang Z, Han B. Chitosan/gelatin–based films crosslinked by proanthocyanidin. Journal of Biomedical Materials Research Part B: Applied Biomaterials. 2005;75(2):442-50.

73. Yu S-H, Wu S-J, Wu J-Y, Peng C-K, Mi F-L. Tripolyphosphate Cross-Linked Macromolecular Composites for the Growth of Shape-and Size-Controlled Apatites. Molecules. 2012;18(1):27-40.

74. Cheung H-Y, Lau K-T, Lu T-P, Hui D. A critical review on polymer-based bio-engineered materials for scaffold development. Composites Part B: Engineering. 2007;38(3):291-300.

75. Zhang Y, Zhang M. Calcium phosphate/chitosan composite scaffolds for controlled in vitro antibiotic drug release. Journal of biomedical materials research. 2002;62(3):378-86.

76. Zhang Y, Ni M, Zhang M, Ratner B. Calcium phosphate-chitosan composite scaffolds for bone tissue engineering. Tissue engineering. 2003;9(2):337-45.

77. Yang C, Xu L, Zhou Y, Zhang X, Huang X, Wang M, et al. A green fabrication approach of gelatin/CM-chitosan hybrid hydrogel for wound healing. Carbohydrate Polymers. 2010;82(4):1297-305.

78. Peter M, Ganesh N, Selvamurugan N, Nair S, Furuike T, Tamura H, et al. Preparation and characterization of chitosan–gelatin/nanohydroxyapatite composite scaffolds for tissue engineering applications. Carbohydrate Polymers. 2010;80(3):687-94.

79. Thein-Han W, Misra R. Biomimetic chitosan–nanohydroxyapatite composite scaffolds for bone tissue engineering. Acta Biomaterialia. 2009;5(4):1182-97.

Chapter VI
Appendix

Materials Science and Engineering C 33 (2013) 4460–4469

Contents lists available at ScienceDirect

Materials Science and Engineering C

journal homepage: www.elsevier.com/locate/msec

Bioactive polymeric–ceramic hybrid 3D scaffold for application in bone tissue regeneration

A.L. Torres [a], V.M. Gaspar [a], I.R. Serra [a], G.S. Diogo [a], R. Fradique [a], A.P. Silva [b], I.J. Correia [a,*]

[a] CICS-UBI — Health Sciences Research Centre, University of Beira Interior, Av. Infante D. Henrique, 6200-506 Covilhã, Portugal
[b] CAST-UBI — Centre for Aerospace Science and Technologies, University of Beira Interior, Calçada Fonte do Lameiro, 6201-001 Covilhã, Portugal

ARTICLE INFO

Article history:
Received 9 May 2013
Received in revised form 29 June 2013
Accepted 5 July 2013
Available online 13 July 2013

Keywords:
3D scaffolds
Bioceramics
Bone regeneration
Foam replication method
Vacuum coating

ABSTRACT

The regeneration of large bone defects remains a challenging scenario from a therapeutic point of view. In fact, the currently available bone substitutes are often limited by poor tissue integration and severe host inflammatory responses, which eventually lead to surgical removal. In an attempt to address these issues, herein we evaluated the importance of alginate incorporation in the production of improved and tunable β-tricalcium phosphate (β-TCP) and hydroxyapatite (HA) three-dimensional (3D) porous scaffolds to be used as temporary templates for bone regeneration. Different bioceramic combinations were tested in order to investigate optimal scaffold architectures. Additionally, 3D β-TCP/HA vacuum-coated with alginate, presented improved compressive strength, fracture toughness and Young's modulus, to values similar to those of native bone. The hybrid 3D polymeric–bioceramic scaffolds also supported osteoblast adhesion, maturation and proliferation, as demonstrated by fluorescence microscopy. To the best of our knowledge this is the first time that a 3D scaffold produced with this combination of biomaterials is described. Altogether, our results emphasize that this hybrid scaffold presents promising characteristics for its future application in bone regeneration.

1. Introduction

Bone is a highly vascularized and dynamic tissue, having extraordinary mechanical properties and intrinsic regenerative capacity [1]. This exceptional characteristic is however rather limited in severe bone traumatisms that involve multiple fractures, bone-associated tumors and degenerative diseases [2]. These are highly debilitating conditions that commonly require medical intervention to restore bone native properties [3].

Currently, several types of biomaterials, such as biofunctional prosthesis [4], injectable substrates [5] and hydrogels [6] are being produced for bone regeneration purposes. Among them, bioactive 3D porous scaffolds are particularly promising for clinical application due to their unique set of characteristics. Scaffolds are porous 3D matrices that act as temporary templates for cell adhesion and proliferation, while providing mechanical support until new bone tissue is formed at the affected area [7]. For this purpose these scaffolds must be produced with materials that promote proper regeneration without eliciting host immune responses or originating toxic metabolites [8]. The 3D features of the template is another critical parameter when therapeutic applications are envisioned, since its spatial architecture should be designed to have interconnected pores that simultaneously induce osteoconductivity of bone-progenitor cells and neovascularization [9]. To further improve and accelerate bone regeneration it is essential that the scaffold is bioactive, i.e., has the ability to form anchoring points with the surrounding bone and soft tissues, stimulating bone growth. Commonly these bonds are formed through an HA-like layer and are responsible for increasing osteointegration and cell growth and differentiation [10].

The desire to gather these complex characteristics into one scaffold is a challenging demand, not only in the design and manufacturing stages, but also in the translation to in vivo applications. In this context, the combination of ceramics with polymers for the synthesis of hybrid scaffolds has been widely investigated in an attempt to mimic bone tissue native structure [11,12]. β-TCP and HA are the most commonly used ceramics since their mineral compositions are similar to those found in human bone [11,13]. Although β-TCP has been extensively used for bone regeneration due to its biodegradability, biocompatibility and osteoconductivity [14,15] its applications to bone tissue regeneration are limited by its poor mechanical properties [16,17].

In different studies bioceramic-based scaffolds have been modified with polymers (as coating or interpenetrating phases) in order to reduce their brittleness and improve mechanical properties [18–21]. In the present study, β-TCP/HA scaffolds were left uncoated or coated with alginate. This polymer is comprised by 1,4′-linked β-D-mannuronic acid and α-L-guluronic acid blocks, which determines alginate physicochemical properties. This natural biomaterial has valuable characteristics, such as biocompatibility, biodegradability, hydrophilicity, low toxicity and gelling capacity with divalent cations [22–25]. In fact, its

* Corresponding author. Tel.: +351 275 329 055.
E-mail address: icorreia@ubi.pt (I.J. Correia).

0928-4931/$ – see front matter © 2013 Elsevier B.V. All rights reserved.
http://dx.doi.org/10.1016/j.msec.2013.07.003

responsiveness to calcium (Ca^{2+})-rich tissue microenvironments, renders it suitable for scaffold coating in bone tissue engineering, as previously reported by our group [26]. Importantly, the ionically cross-linked alginate mechanical strength rises with increasing divalent ion concentration, and also when these ions have high affinity for alginate [27]. Due to these valuable characteristics, this polymer has been widely used in biomedical applications, including cell encapsulation [28] and drug loading and delivery [29].

In this context, this work reports the production of β-TCP/HA scaffolds by the foam replication method (FRM), followed by their coating with alginate. The scaffold production method used is simple, cost-effective, excludes the use of organic solvents and, most importantly, allows the manufacture of reproducible structures. Three types of scaffolds with different β-TCP:HA ratios and alginate coatings were developed and their physicochemical and biological properties investigated.

2. Materials and methods

2.1. Preparation of β-TCP/HA composite scaffolds followed by alginate coating

β-TCP/HA scaffolds were produced using a polymer-based FRM, which allows the control of the dimensions, pore size and density of the 3D scaffold. Three different types of scaffolds were prepared, concerning the quantity of β-TCP (Panreac®) relatively to HA nanopowder (<200 nm particle size, Sigma-Aldrich): 80/20% (w/w), 90/10% (w/w) and 99/1% (w/w), respectively. Poly(vinyl) alcohol (PVA) (Sigma-Aldrich) (β-TCP binder agent) was added to the polymer mixture in a ratio of 1:10 (% w/w) PVA:β-TCP. Briefly, to prepare the polymer blends, PVA was dissolved in 15 mL of deionized water, under constant stirring, for 30 min, at 50 °C. Then, both β-TCP and HA powders were added in small amounts to the solution, under constant stirring at room temperature (RT). After all the powder was wetted, the mixture was sonicated for 15 min. The used polyurethane (PU) foams had similar structures to that of the human cancellous bone and were cut ($5 \times 5 \times 5$ mm^3) to be used as a sacrificial template for the FRM. All the PU foams were cleaned in a 0.1 M sodium hydroxide (NaOH) (Sigma-Aldrich) solution, followed by rinsing twice with distilled water before air-dried for 12 h. The PU foams were then repeatedly immersed in the polymer blends in order to promote polymer penetration into the PU foam pores. The PU foams impregnated with the polymer blends were then gently squeezed to remove the excess of the slurry. Homogeneous coating of the PU foams with β-TCP/HA was possible after several immersions. The coated PU foams were exposed to air, allowed to dry overnight, at RT, and then sintered. Briefly, the PU-polymer foams were step-wise heated in a furnace at 1 °C/min to 900 °C and then kept at this temperature for 240 min. Additionally, some of the 3D scaffolds were subsequently coated with a 2% sodium alginate (Sigma-Aldrich) solution, (molecular weight (Mw) 120.000–190.000 Da), under vacuum at RT, for 30 min, in order to guarantee alginate inclusion within the scaffold pores. These coated scaffolds were then immersed in a 5% calcium chloride ($CaCl_2$) solution (Sigma-Aldrich), under vacuum for 10 min, in order to cross-link alginate-coated scaffolds. The structures were maintained in the $CaCl_2$ solution for 24 h and then air dried, prior to use. From this point onwards alginate coated β-TCP/HA scaffolds are identified as: 80/20/A, 90/10/A and 99/1/A and the uncoated scaffolds as 80/20, 90/10 and 99/1.

2.2. Chemical, mechanical and morphological characterization of the β-TCP/HA composite scaffolds

2.2.1. Fourier transform infrared spectroscopy

The physicochemical characteristics of the manufactured 3D scaffolds were evaluated by Fourier transform infrared spectroscopy (FTIR) by using a Nicolet iS10 interferometer (Thermo Scientific, Waltham, MA, USA). Briefly, samples were mounted on a diamond window and compressed to improve spectrum signal to noise ratio. For each sample, 128 interferograms were acquired with a spectral width ranging from 4000 to 400 cm^{-1} and a spectral resolution of 4 cm^{-1}. The acquired data was then processed in Omnic Spectra analysis software, where baseline subtraction was performed.

2.2.2. Energy dispersive spectroscopy

Energy-dispersive X-ray spectroscopy (EDS) (Rontec) was used for the elementary characterization of both, coated and uncoated, β-TCP/HA scaffolds. Prior to all analyses, samples were placed on an aluminum stub support, air-dried at RT and sputter-coated with gold.

2.2.3. Resistance to compression, fracture toughness and Young's modulus

To characterize the mechanical behavior of the cuboid-shaped coated and uncoated scaffolds, uniaxial compression tests were performed. All the measurements were performed at RT using a Zwick® 1435 Material Prüfung (Ulm, Germany) with a crosshead speed of 0.2 mm/min and a load cell of 5 kN. Four specimens from each sample were tested and their dimensions acquired. Afterwards, compressive strength (Cs) of each type of scaffold was calculated by applying Eq. (1) [30].

$$\mathrm{Cs} = \frac{F}{a \times l} \tag{1}$$

where F is the load at the time of the fracture and a and l represent the width and length of the scaffold, respectively. The fracture toughness (FT) and Young's modulus (YM) were estimated from the stress–strain relations calculated and applying Eqs. (2) and (3), respectively [31,32].

$$\mathrm{FT} = \frac{Hd \times \mathrm{Cs}}{2} \tag{2}$$

$$YM = \frac{\mathrm{Cs}}{Hd} \tag{3}$$

where Hd is the scaffold height deformation and Cs is the scaffold compressive strength. Average values and standard deviations (s.d.) were determined for each sample as previously described in the literature [33].

2.2.4. Scanning electron microscopy

In order to assess scaffold morphology, porosity and cellular behavior in the presence of the samples, scanning electron microscopy (SEM) analysis was performed. Samples were washed at RT with phosphate buffer solution (PBS, pH 7.4) (Sigma-Aldrich) and fixed for 30 min with 2.5% (v/v) glutaraldehyde (Sigma-Aldrich) diluted in a 0.1 M sodium cacodylate solution (Sigma-Aldrich). Then, samples were washed three times with cacodylate buffer and finally incubated for 10 min in a graded series of ethanol solutions (50, 60, 70, 80, 90 and 99% v/v), for dehydration. Scaffolds were then stored in absolute ethanol, at 4 °C, until being subjected to CO_2 critical point drying, mounted onto aluminum stubs with araldite glue and sputtered-coated with gold using an Emitech K550 sputter coater (London, UK). SEM images were obtained with a scanning electron microscope Hitachi S-2700 (Tokyo, Japan) with an acceleration voltage of 20 kV at suitable magnifications.

2.2.5. Porosity evaluation

The total porosity (P) of the different types of β-TCP/HA scaffolds, was determined by following a method described elsewhere [34]. The amount of absolute ethanol that the scaffolds were able to absorb in 24 h, was determined by applying Eq. (4).

$$\mathrm{P}(\%) = \frac{W_2 - W_1}{d_{\mathrm{ethanol}} \times V_{\mathrm{scaffold}}} \times 100 \tag{4}$$

where W_1 and W_2 are the weights of the dry and the wet scaffolds, respectively, d_{ethanol} is the density of the ethanol at RT and V_{scaffold} is the

volume of the wet scaffold, directly determined by immersion. For each scaffold, three replicates were analyzed and data represents the average of each replicate.

2.2.6. Contact angle measurements

The contact angle measurements of the samples were performed using the sessile drop technique and water was used as reference fluid [35]. Contact angle data was acquired in a Data Physics Contact Angle System OCAH 200 apparatus, operating in static mode at RT. For each sample, water drops were placed at various locations of the analyzed surface.

2.3. Biological characterization of the β-TCP/HA composite scaffolds

2.3.1. Culture of human osteoblasts in the presence of the scaffolds

Human osteoblasts (CRL-11372), purchased from American Type Culture Collection, were cultured in Dulbecco Modified Eagle Medium, Nutrient Mixture F-12 (DMEM-F12) (Sigma-Aldrich), supplemented with 10% heat inactivated fetal bovine serum (FBS) (Biochrom AG), streptomycin (Sigma-Aldrich) (100 μg/mL) and gentamicin (Sigma-Aldrich) (100 μg/mL), in 75 cm^2 T-flasks (Orange Scientific). Cultures were maintained at 37 °C in a 5% CO_2 humidified atmosphere and the culture medium exchanged twice a week. Confluent cell monolayers were subcultured by initially washing them with PBS, and then detached with 0.18% trypsin (1:250) and 5 mM EDTA (Sigma-Aldrich). A Neubauer chamber was used to determine cell number using trypan blue (Sigma-Aldrich) — exclusion assay, in order to distinguish live from dead cells. Subsequently, cells were seeded in contact with 80/20, 90/10, 99/1, 80/20/A, 90/10/A and 99/1/A scaffolds at a density of 2.0×10^3 cells/well in cell culture treated polystyrene plates. Cell growth was monitored during 1, 7 and 14 days, by using an Olympus CX41 inverted light microscope (Tokyo, Japan) equipped with an Olympus SP-500 UZ digital camera.

2.3.2. Cellular metabolic activity: resazurin assay

Osteoblast cells were cultured on scaffold surfaces for 1, 7 and 14 days. A non-toxic dye, specifically, resazurin (Sigma-Aldrich) was used to assess cellular metabolic activity during this period. Resazurin is reduced to a fluorescent resorufin substrate by an intracellular enzyme, specifically oxidoreductase. At the indicated time points of culture, 400 μL of culture medium was added to the wells with 40 μL of a 10% (v/v) fluorescent dye solution and incubated for 4 h, in a humidified atmosphere, at 37 °C, 5% CO_2. Then, 80 μL of the supernatant was transferred into a 96-well plate and the fluorescence intensity measured in a SpectraMax Gemini™ XS spectrofluorometer (Molecular Devices), at $\lambda_{ex} = 545$ nm and $\lambda_{em} = 590$ nm, respectively. Cells cultured without scaffolds were used as negative control and ethanol treated cells were used as positive control.

2.3.3. Analysis of 3D scaffolds biologic properties

The analysis of osteoblast adhesion and morphology on the 3D scaffold surfaces at various days (1, 7 and 14) was visualized by fluorescence confocal laser scanning microscopy (CLSM). Briefly, at pre-determined time points the cell culture medium was removed and cells were washed three times with PBS at RT. The remaining cells were then fixed with 4% paraformaldehyde (PFA) (Sigma-Aldrich) for 30 min, at RT, and were washed once more with PBS to remove PFA. Afterwards, the cell nucleus was labeled with 2 μM propidium iodide (Molecular Probes, Invitrogen, Carlsbad, MO, USA) solution during 15 min, at RT, followed by five additional washes with PBS. Furthermore, propidium iodide stained cells were also permeabilized with 1% Triton X-100 (Sigma-Aldrich) and then blocked with blocking solution (10% FBS, 0.1% Tween (Sigma-Aldrich)) in PBS, for 10 min. Afterwards, cells were incubated with mouse anti-β-actin antibody (Molecular Probes, Invitrogen) (1:500) for 1 h at RT in a humidified chamber. Following the incubation period osteoblasts were thoroughly washed with PBS-T (0.1% Tween in PBS). The anti-mouse Alexa-488 (Molecular Probes, Invitrogen) antibody was then added to cells during 1 h, followed by the washing steps as previously described. The cell-seeded scaffolds were then transferred into μ-Slide 8 well Ibidi® chamber coverslips (Ibidi® GmbH, Germany) and imaged in a Zeiss LSM 710 confocal microscope (Carl Zeiss SMT Inc., USA) equipped with a Plan-Neofluar 10×/NA 0.3 and a Plan-Apochromat 40×/1.4 Oil DIC objectives. All data was

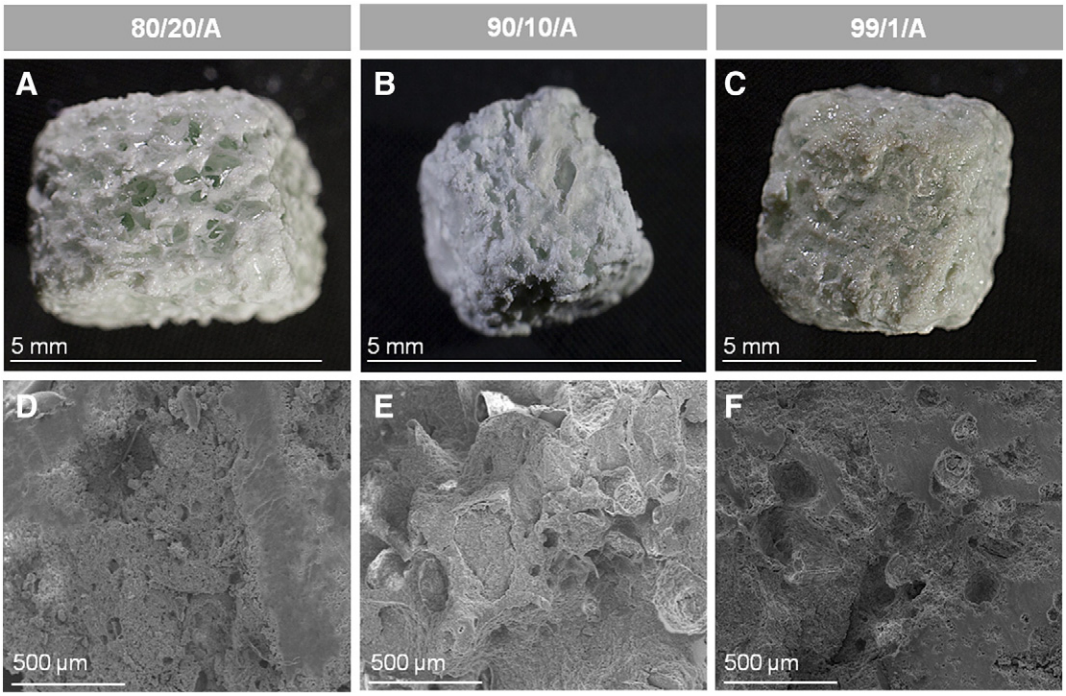

Fig. 1. Macrographs (A, B and C) and SEM images (D, E and F) of the different alginate-coated β-TCP/HA scaffold surfaces. Images show the surface characteristics and the porosity of the 80/20/A (A, D), 90/10/A (B, E) and 99/1/A (C, F) 3D scaffolds, respectively.

Table 1
Pore diameter and hydrophilic properties of the produced β-TCP/HA 3D scaffolds.

Scaffold	Pore diameter (μm)		Contact angle
	Minimum	Maximum	
80/20	80	450	[a]
80/20/A	60	250	20.6°
90/10	90	280	17.2°
90/10/A	30	160	21.6°
99/1	80	125	20.4°
99/1/A	60	115	26.6°

[a] Lower than the quantification limit.

acquired in z-stack mode with a step of 4.67 μm. Z-stacks were then rendered into 3D images in the Zeiss LSM 710 software. Depth coding rendering of z-stacks was also performed in Zeiss software with the open GL rendering mode to provide visualization of cell spatial distribution within the scaffold architecture. Additional image processing was performed in Image J (ImageJ software) [36].

2.4. Statistical analysis

Comparison of the results obtained for the different groups of scaffolds at various conditions was performed by using one-way analysis of variance (ANOVA), with the Newman–Keuls post-hoc test [37]. This statistical test is applied to compare the mean and the differences among three different groups [38]. Thus in this particular case the ANOVA test was used to evaluate the differences in the means of three samples of different scaffold formulations by using variances. This test was performed by taking into consideration that the samples are independent from each other and that the variance of the populations is equal. The addition of the post-hoc Newman–Keuls test was used to further provide a more detailed analysis of differences in the means by making a multi-pairwise comparison [39]. A p value below 0.05 ($p < 0.05$) was considered statistically significant.

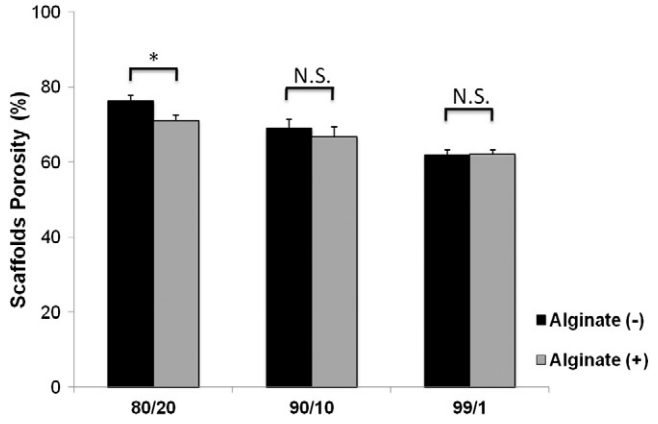

Fig. 2. Total porosity of the different β-TCP/HA scaffolds. Alginate (+) indicates coated scaffolds and alginate (−) the uncoated scaffolds. N.S.: not significant; *$p < 0.05$, $n = 3$.

3. Results and discussion

In this study the physicochemical, mechanical and biological characteristics of 3D porous scaffolds produced with two bioceramics, β-TCP and HA, were investigated. So far, two ratios of β-TCP and HA were successfully tested in humans, specifically, 50/50 and 40/60 [40,41]. Herein, the use of higher percentages of β-TCP relatively to HA was evaluated to produce scaffolds with improved mechanical properties for bone regeneration.

Furthermore, an alginate coating was added to the scaffolds to include an additional biomaterial that could mimic the extracellular matrix present in native bone cells, and also that would enhance the mechanical strength of the structure, improving its osteoconduction and osteointegration within host bone tissues [42]. Alginate was also chosen to be included in this study since its combination with β-TCP and HA forms a rigid hybrid polymer–ceramic biomimetic composite, without eliciting any immune response, or risk of contamination by allo- or xeno-proteins or viruses, unlike, for instance, collagen [43]. Furthermore, the FRM method used to produce the 3D structures allows the production of interconnected porous scaffolds with rough surfaces, with controllable pore size and porosity within the template geometry [44–46].

3.1. β-TCP/HA composite scaffold production: macroscopic, mechanical and physicochemical characterization

As previously described in the literature, scaffolds produced for bone tissue regeneration must have adequate external and internal structures, as well as desirable physicochemical characteristics that mimic the extracellular matrix of bone cells and also bone native properties. The uncoated β-TCP/HA (Supplementary Fig. 1) and alginate-coated β-TCP/HA scaffolds (Fig. 1) produced by FRM have well defined

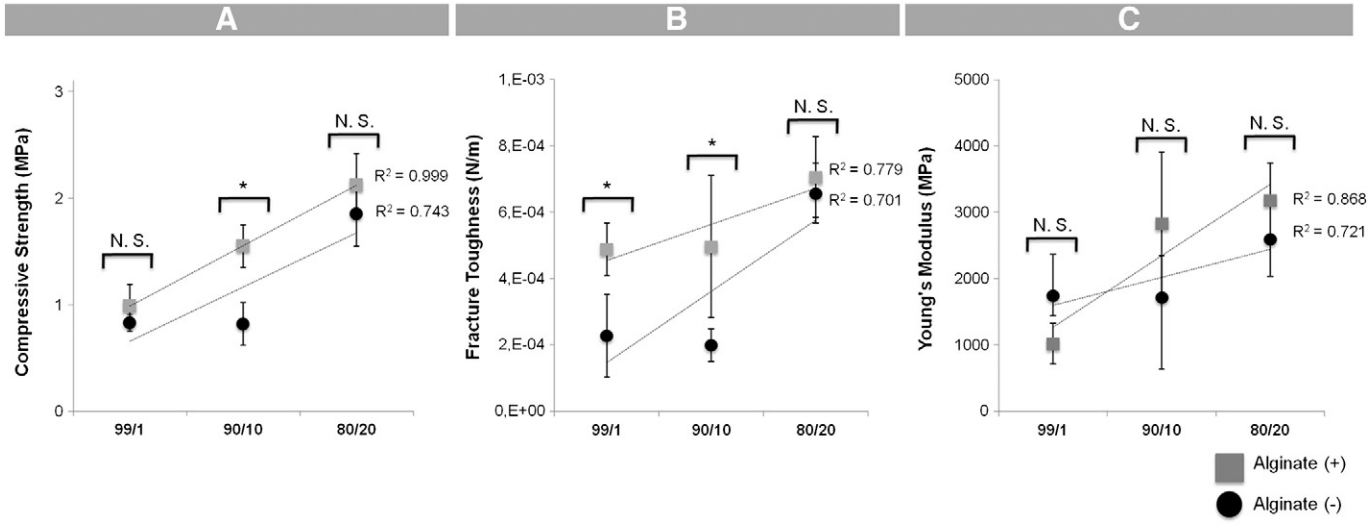

Fig. 3. Compressive strength (A), fracture toughness (B) and Young's modulus (C) of the uncoated (gray squares) and alginate-coated (black circles) 80/20, 90/10 and 99/1 scaffolds. N.S.: not significant; *$p < 0.05$, $n = 3$.

Table 2
Comparison of the mechanical properties between the 80/20/A scaffold and the human cancellous bone.

Mechanical properties	80/20/A scaffold	Human cancellous bone
Compressive strength	2.12 ± 0.30 MPa	2.00–12.00 MPa
Fracture toughness	$7.06 \times 10^{-4} \pm 1.22 \times 10^{-4}$ N/m	0.11 N/m
Young's moduli	3181.00 ± 561.93 MPa	100.00–500.00 MPa

architectures that replicate those of their sacrificial foam templates. Interestingly, although the β-TCP and HA components of bone substitutes were different among the tested scaffolds, all of them presented surfaces with some degree of roughness, even after being coated with alginate. These findings assume further importance since roughness largely influences protein adsorption and cell adhesion upon scaffold implantation [47]. In fact, as recently reported by Gittens and co-workers [48], micro- and macro-sized topographic surface roughness of bone substitutes improves osteoblast differentiation and localized growth factor production, thus enhancing scaffold osteointegration in bone defects [48]. Moreover, SEM analysis confirmed the presence of micro- and macro-porosity throughout the alginate-coated (Fig. 1) and the uncoated scaffolds (Supplementary Fig. 1).

The results presented in Table 1 revealed that the 80/20 formulation has the larger sized pores when compared to the 90/10 and 99/1 scaffolds. After performing the alginate coating, a clear decrease in the pore size was observed, in comparison with their uncoated counterparts (Table 1). Nevertheless, all the coated scaffolds maintained suitable pore diameters for use in bone regeneration, with the 80/20/A structure being the one with larger pores. Such is of crucial importance, since pore diameters ranging from 100 μm to 135 μm have shown to improve osteoblast-bone deposition and formation of rich vascular networks [49].

Furthermore, other important physicochemical properties, such as hydrophilicity and total percentage of porosity of the scaffolds, influence their bioactivity and regenerative capacity. As shown in Table 1 the measured values of the contact angles for the 90/10 and 99/1 scaffolds, indicate that these templates are highly hydrophilic. It is important to mention that the contact angle of the 80/20 scaffold could not be calculated, due to the rapid absorption of the water drop by the porous structure, suggesting that this scaffold is highly hydrophilic. However, after performing alginate inclusion, it was possible to determine the 80/20/A contact angle and it was found that this value is quite low, suggesting that, even after its coating, this scaffold remains as the most hydrophilic of the three coated scaffolds (Table 1). Although the contact angle values of the alginate-coated structures suffered a slight increase when compared to the respective uncoated ones, they remained in the range of hydrophilic associated angles, suggesting that these structures were also hydrophilic. These results indicate that cellular adhesion and migration within the 80/20/A might occur in an improved manner, since this scaffold is highly hydrophilic, and the presence of alginate may create additional biomimetic substrates between the pores, increasing the available areas within the scaffolds for cells to migrate.

The total percentage of scaffold porosity was determined by a liquid displacement method, using ethanol as the displacing liquid [50]. By analyzing Fig. 2, it is possible to observe that all the scaffolds present an internal porosity higher than 60%, a suitable value for bone regeneration, considering that the human cancellous bone bears a total porosity of 30% to 90% [51]. More importantly, the 80/20 scaffold presents the higher value of porosity (76%), when compared to the 90/10 and 99/1 scaffolds. These results corroborate the previous findings concerning the diameter of the pores and the contact angles. Such results may, at first glance, seem to be in contradiction with those previously published in the literature [52,53]. These researchers reported that porosity is inversely proportional to HA concentration. Furthermore, Muralithran and collaborators, have previously reported that by increasing the sintering temperature (from 1000 °C to 1450 °C), the relative density and linear shrinkage of HA ceramics increase and consequently the porosity decreases [54]. In this study a 900 °C temperature was used in the sintering process, which could influence the porosity results. Moreover, the increase in scaffold porosity with a higher HA (w/w) content in the scaffolds may be explained by the fact that there is a larger relative concentration of smaller sized particles in respect to those of β-TCP (HA nanoparticles < 200 nm, β-TCP mean particle size 11.64 μm). In fact, particle size has been shown to affect total porosity since as described

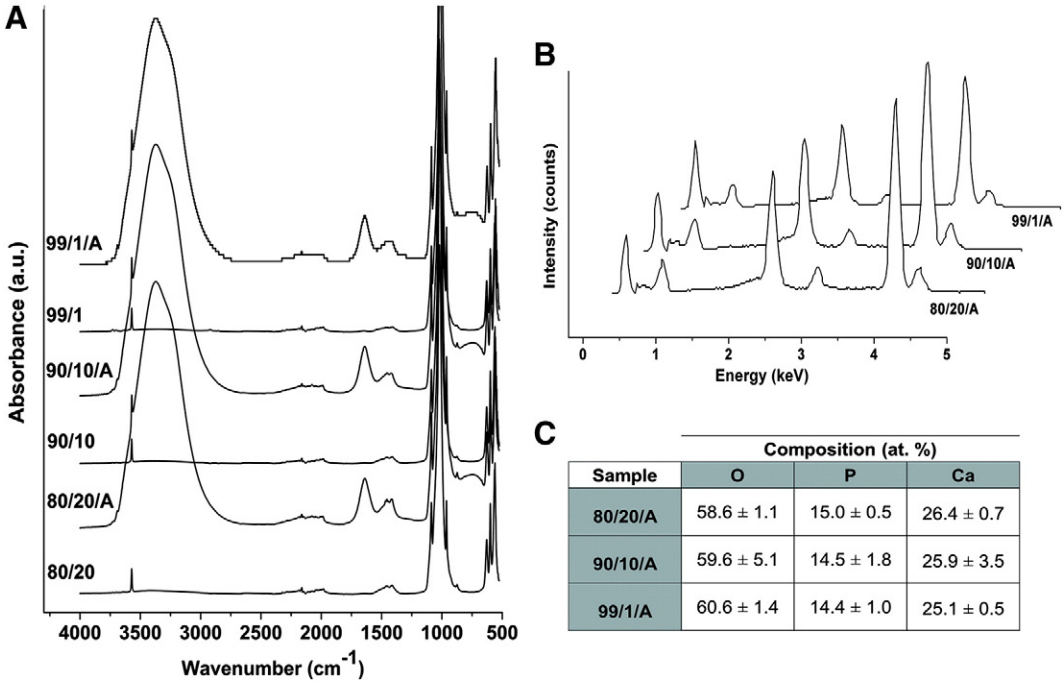

Sample	Composition (at. %) O	P	Ca
80/20/A	58.6 ± 1.1	15.0 ± 0.5	26.4 ± 0.7
90/10/A	59.6 ± 5.1	14.5 ± 1.8	25.9 ± 3.5
99/1/A	60.6 ± 1.4	14.4 ± 1.0	25.1 ± 0.5

Fig. 4. Physicochemical characterization of the powders and 3D scaffolds. (A) FTIR spectra, (B) EDS spectra of the 3D scaffolds and (C) elemental analysis of the manufactured structures.

through molecular dynamics simulations performed by Balakrishnan et al. [55], the formation of agglomerates is dependent on the application of higher forces to compact nanoparticles [55]. Therefore, since no forces were applied to form compact nanoparticle aggregates the more space occupied by HA powders in 80/20 scaffolds, presents higher interfacial voids, and thus, increased total porosity. It is also important to emphasize that an increased HA concentration increases the viscosity of the slurry, a fact that will lead to highly porous materials after sintering as reported by Sopyan et al. [56]. Thus the increasing porosity in the 80/20 scaffold in comparison with the other formulations may also be correlated with the higher viscosity promoted by HA.

Regarding the scaffold porosity after the coating procedure, a slight decrease (5%) was observed for the 80/20/A template in comparison with the respective uncoated scaffold. Even though, this scaffold was also the most porous in comparison with all other coated ones (Fig. 2). The existence of pores is fundamental as it promotes nutrient intake, as well as, interactions between the β-TCP/HA template and bone cells. The establishment of this microenvironment promotes cell attachment, migration and proliferation in a 3D area [57–59]. Apart from pore size, pore interconnectivity is also a desirable characteristic due to its important influence on cell proliferation and differentiation [60]. In fact, interconnected pores facilitate the formation of vascular networks within the 3D scaffolds and provide channeling pathways for biofluids [61]. These biofluids promote the adsorption of Ca^{2+} and PO_4^{3-} ions throughout the biomaterial, creating an HA-like layer [10]. This layer establishes an interface between the implant and the 9 surrounding bone tissues and stimulates osteoblast cell activity, increasing the deposition of bone matrix in the defect area. Additionally the formation of this layer increases the osteoconductivity and osteointegration, further contributing for the bone mineralization [17].

Achieving equilibrium between scaffold porosity and adequate mechanical strength, is a demanding objective for the production of scaffolds, as it was taken into consideration in this study. The mechanical behavior of the 3D scaffolds was characterized by analyzing their resistance to compression, followed by an estimation of the values of fracture toughness and Young's modulus. Through the analysis of Fig. 3 it is possible to visualize that the compressive strength, the fracture toughness and the Young's modulus of the 80/20 scaffold are higher than the values of the 90/10 and 99/1 scaffolds. With increase of porosity (99/1 to 80/20) there is an increase in the mechanical strength by 2 times. This improvement in mechanical compression strength is due to the increasing densification of the walls due to the increase of the amount of HA. This is also corroborated by the increased material stiffness (highest Young's modulus). After coating the scaffolds with a 2% alginate solution their mechanical properties improved, with the 80/20/A maintaining better mechanical resistance to compression, resistance to fracture and elasticity modulus than the other coated 3D structures. Accordingly, it was previously described that an increase in the volume fraction of alginate from 1 to 3% results in an improvement of the compressive modulus [62]. So, it is noticeable that the most porous structures (80/20 and 80/20/A) are also those with better mechanical properties, when compared to both the uncoated and coated 90/10 or 99/1 scaffolds. These findings are likely correlated with the fact that the 80/20 and 80/20/A scaffolds have higher amounts of HA and lower quantities of β-TCP, in comparison to the other manufactured scaffolds. This is consistent with a study performed by Shiota, T. et al., that revealed that high amounts of β-TCP are responsible for a decrease in scaffold strength resistance [63]. Comparing the mechanical properties of 80/20/A scaffold with those presented by the natural cancellous bone, it is possible to observe that this scaffold is the most promising for therapeutic applications, among the scaffolds produce herein (Table 2) [64–66].

The different scaffolds produced by FRM were then characterized by FTIR spectroscopy. The stretching bands obtained between 500 and 600 cm^{-1} for the manufactured structures are characteristic of the PO_4^{-} ions present in both β-TCP and the HA powder (Fig. 4A). The stretching of the –OH groups was also observed (3571 cm^{-1} and libration mode at ≈630 cm^{-1}). This particular band intensity is higher in all the synthesized scaffolds, since it is the end result of the cumulative contribution of both HA and β-TCP (Fig. 4A). In addition, the stretching bands observed at ≈1415 and 1450 cm^{-1} are attributed to a B type apatite [67]. Furthermore, EDS analysis of the scaffolds shows that the chemical composition of all the alginate coated formulations is very similar in terms of phosphate and calcium (Fig. 4C).

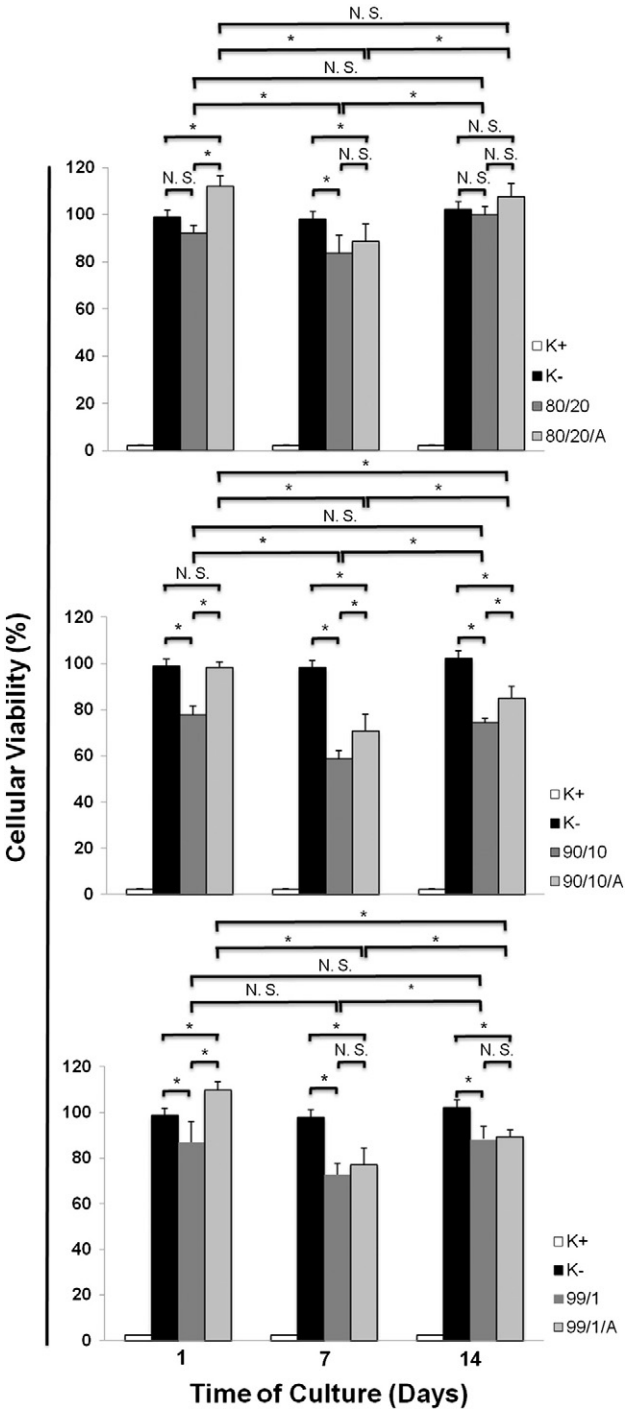

Fig. 5. Osteoblast cell metabolic activity when cultured in the presence of different β-TCP/HA scaffolds. Cultures were evaluated for 1, 7 and 14 days. K^+ and K^-, indicate dead and viable cells, representing positive control and negative control, respectively. N.S.: not significant; *$p < 0.05$, $n = 3$.

3.2. Analysis of the biological properties of the scaffolds

Subsequently, the biological performance of the porous β-TCP/HA structures was also evaluated. For this purpose, human osteoblast cells were cultured in the 3D scaffolds for up to 14 days and their metabolic activity evaluated at the indicated time points (Fig. 5). The results obtained revealed that osteoblast metabolic activity when cultured in the presence of all the scaffolds was higher than 70% during the 14 days of analysis, indicating that the 3D bioceramics are biocompatible. Among all the uncoated scaffolds, the 80/20 formulation was the one that presented higher biocompatibility along the assay and comparatively to 90/10 and 99/1 scaffolds. Cells presented higher metabolic activity in the presence of alginate coated-β-TCP/HA scaffolds than in contact with uncoated scaffolds ($p < 0.05$). The 80/20/A structure was the one for which cells presented the higher viability, being close to the value presented by the negative control for all culture days (approximately 100%).

To further characterize cellular adhesion both on the surface and inside the scaffold, SEM analysis was performed and it showed that osteoblasts were able to adhere preferably inside the pores of the bioceramic scaffolds, either coated (Fig. 6) or not (Supplementary Fig. 2) with the natural polymer. Interestingly, after the first day in contact with the scaffolds, osteoblasts were already attached and spread across the 3D structures, presenting a round shape configuration, with some cytoplasm extensions towards the substrate. At day 7, and predominantly after 14 days of culture, cells cultured in all the different structures started to present a typical osteoblastic morphology, showing a smooth arrangement with more lamellipodia connecting to surrounding osteoblast, beginning to form a continuous cell layer. For all the uncoated and coated β-TCP/HA scaffolds, the number of osteoblasts appeared to increase along time, with cells establishing connection areas between them. SEM analysis was also important to investigate whether alginate was or not occluding the pores of the coated scaffolds and if cells were still able to migrate within these scaffolds. As depicted in Fig. 6, alginate did not block the pores, but instead created additional biocompatible substrates, changed the roughness and microtopography of the scaffolds surface, which contributed to further increase osteoblast adhesion and migration. These results are further emphasized by the CLSM analysis during the various stages of osteoblast contact with the scaffolds (Fig. 7). In fact, as shown in Fig. 7, during osteoblast contact with the alginate-coated 3D scaffolds, cells were able to adhere and proliferate in all bioceramic formulations, emphasizing their biocompatibility and suitable physicochemical properties to promote osteoblast adhesion. These findings were also observed for the uncoated bioceramic scaffolds. Furthermore, at days 7 and 14 it is clear that osteoblasts migrate into the porous network during the time course of incubation. A visual analysis of the orthogonal slices of the scaffolds also clearly demonstrates that osteoblasts are spread across the entire scaffold and are also located inside the scaffold pores.

To further visualize the cytoplasmic morphology and localization of the osteoblasts that were proliferating on the 3D hybrid scaffolds an immunocytochemistry analysis of β-actin was performed. As the CLSM 3D reconstruction images demonstrate, osteoblasts present their characteristic cytoplasmic morphology for all scaffolds (Fig. 8).

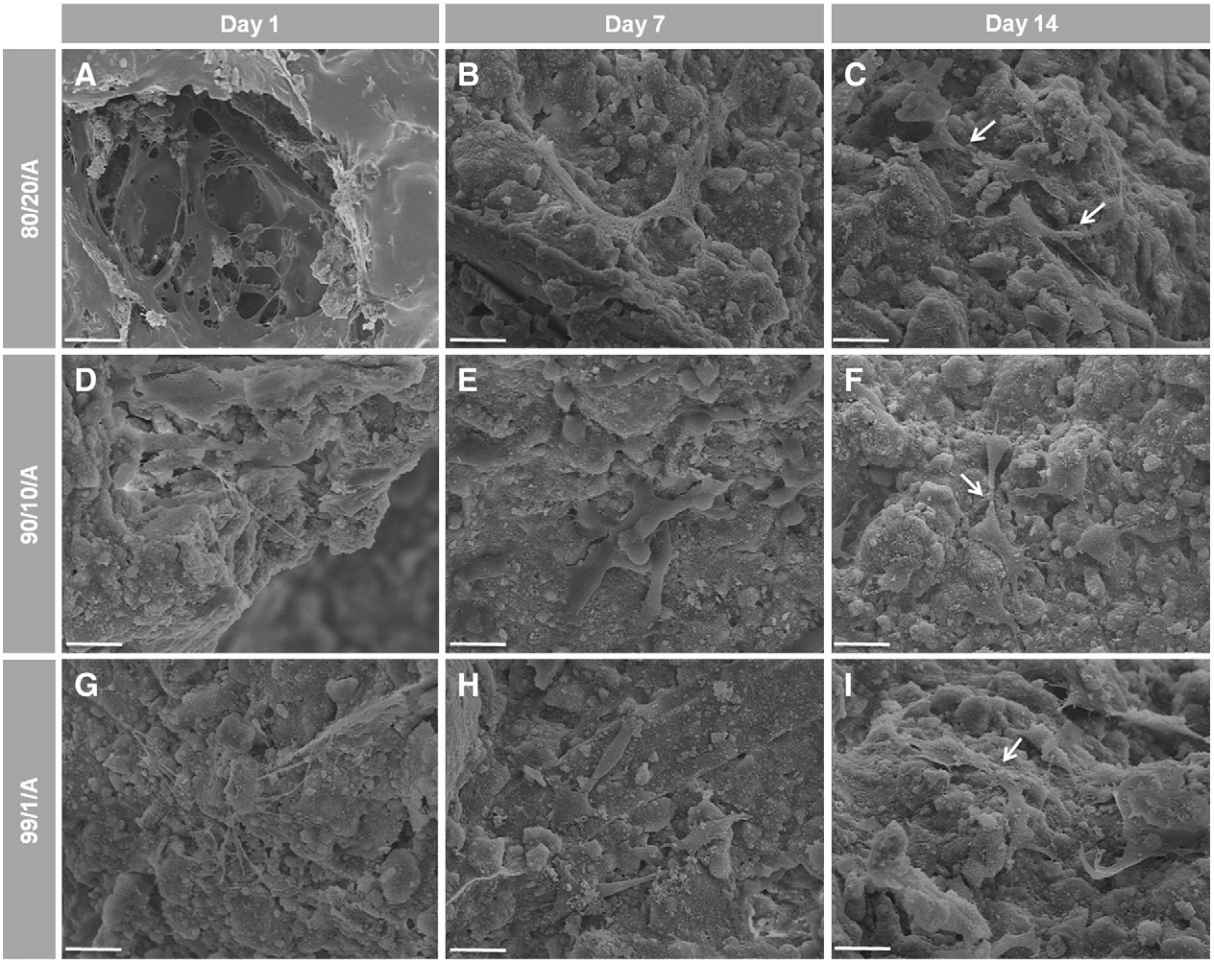

Fig. 6. SEM micrographs of osteoblast morphology in the presence of the different β-TCP/HA/alginate scaffolds. SEM images were used to visualize osteoblasts on the surface of the 80/20/A (A, B and C), 90/10/A (D, E and F) and 99/1/A (G, H and I) 3D scaffolds, at culture days 1 (A, D and G), 7 (B, E and H) and 14 (C, F and I). Scale bars correspond to 20 μm.

In addition, color coded depth analysis of the alginate coated structures clearly shows that osteoblasts are capable of migrating and attaching into deep sections of the scaffolds with some cells being localized up to 300 μm within the pores (Fig. 8). This is a relevant finding since the deposition of bone matrix inside the scaffold will eventually fill the bone defect while the scaffold is biodegraded, restoring the structure and function of the native bone.

Together, our results demonstrate that the produced β-TCP/HA structures are highly porous, hydrophilic, biocompatible and resistant to compression, improvements particularly achieved for the 80/20 structure. It was also shown that a mixture of β-TCP and HA, has the benefit of combining the bioactivity of β-TCP and the stability of HA. Moreover, higher amounts of HA increased the scaffold mechanical strength, while smaller amounts of β-TCP led to an increase of structure porosity. Besides, this study also reveals that the combination of both β-TCP and HA improves the biological and mechanical properties, in comparison with previously developed scaffolds comprised of β-TCP or HA alone [68–70]. In fact, the combination of these bioceramics originated 3D porous and bioactive structures with desirable osteoconductive and osteoinductive properties. Our novel approach involving an additional alginate coating further improves the scaffold mechanical, physicochemical and biological properties, as this natural biopolymer bridges the gap between the required material properties and bioactivity for therapeutic applications. Overall, the manipulation of bioceramic–polymer relative ratios largely influenced all the 3D scaffold properties and led to the manufacture of a particularly improved formulation with suitable characteristics for repair (Table 3, 80/20/A formulation). The role of alginate in the improvement of the mechanical properties is even more evident when comparing the scaffolds herein presented with those produced by Ebrahimi, M. et al. [31], which describes the production of β-TCP and HA scaffolds coated with collagen. An analysis of both types of scaffolds reveals the superior contribution of alginate, when compared to collagen, for the improvement of the scaffold mechanical strength and because, unlike collagen, alginate does not represent a risk of disease transmission [43]. Considering that the in vivo performance of β-TCP and HA has already been tested in humans [40,41], from this standpoint we envision that the addition of this polymer may actually improve the clinical outcome of these biomaterials.

4. Conclusions

In this work we describe the manufacture of 3D tunable porous scaffolds for bone regeneration by using a cost-effective and reproducible technique. Our results revealed that by optimizing the ratios of different bioceramic composites in the scaffolds the physicochemical and biological properties of these 3D constructs could be improved. In addition, the method employed for template production, allows the synthesis of scaffolds with rough topographies, micro- and macro-pores that are homogeneously distributed in the scaffold 3D volume. Furthermore, in order to improve the overall performance

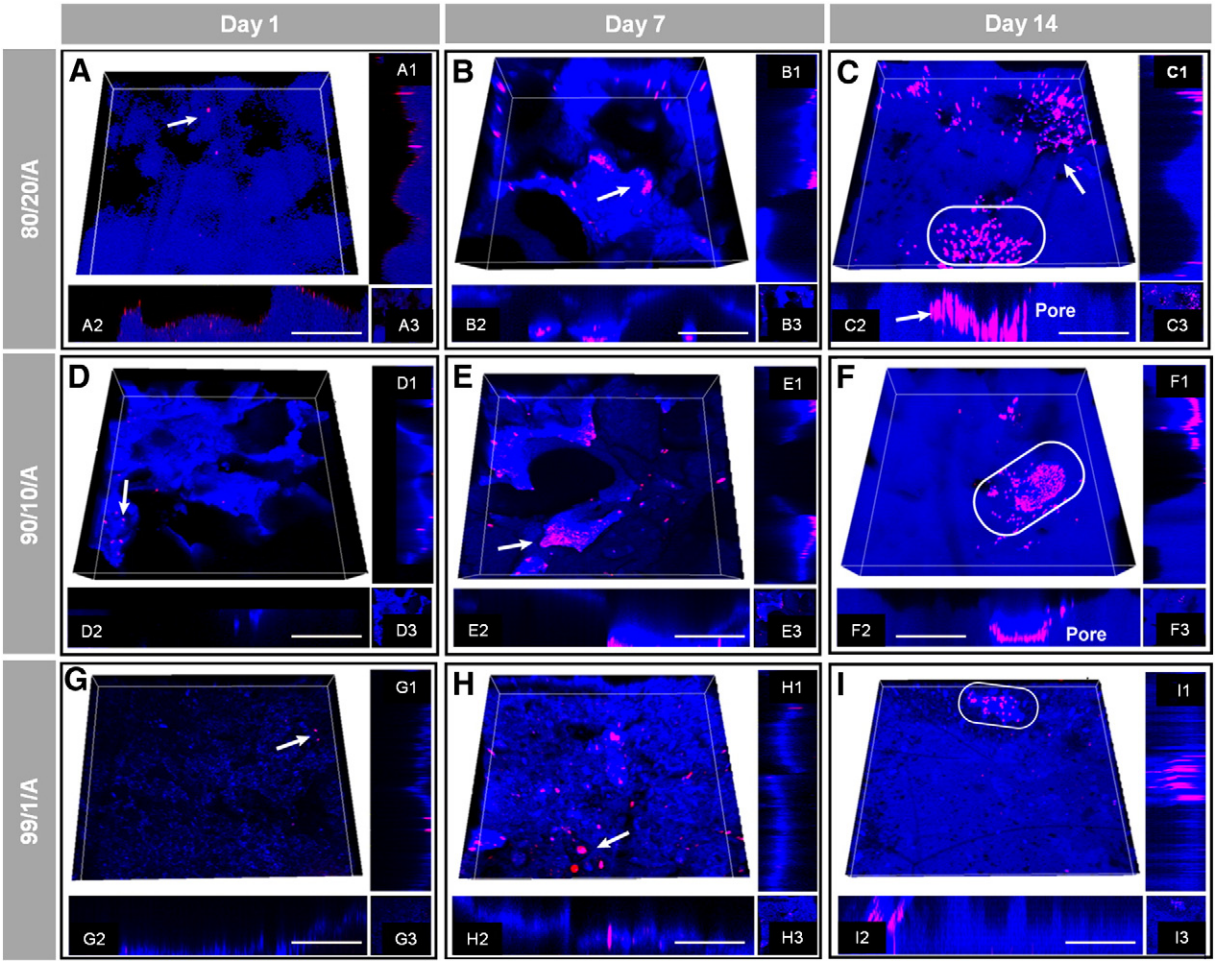

Fig. 7. Osteoblasts are able to attach to the surface of the different scaffolds. Confocal microscopy images were used to investigate osteoblast distribution on the alginate coated scaffolds at different time points. (A to I) 3D reconstruction of the hybrid scaffolds; (A1 to I1) Orthogonal slices of scaffold xx axis. (A2 to I2) Orthogonal slices of scaffold yy axis. (A3 to I3) Top view of the 3D scaffolds. Red channel: cell nucleus; blue channel: 3D scaffolds. White arrows indicate cells. White ovals indicate pores. White scale bars represent 300 μm.

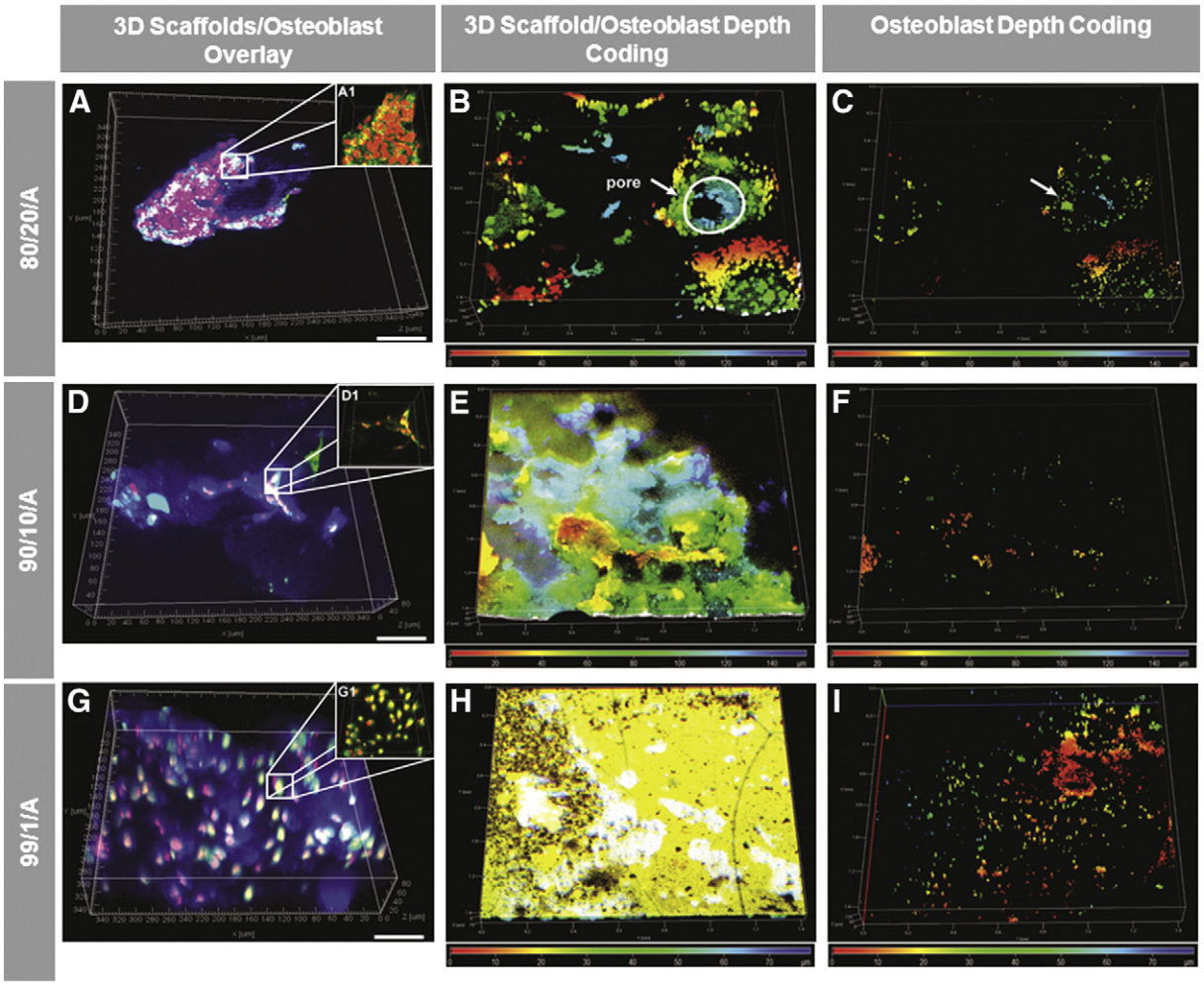

Fig. 8. 3D reconstruction and depth analysis of the different scaffolds coated with alginate. (A, D and G) Immunocytochemistry analysis of osteoblast seeded scaffolds at day 14. Green channel: β-actin; red channel: cell nucleus; blue channel: 3D hybrid scaffolds. (B, E and H) 3D depth coding of scaffolds and osteoblasts cultured on scaffold's surface. Size bar represents color-coded depth. White area represents a scaffold pore with osteoblasts inside. (C, F and I) 3D surface reconstruction of cells at the surface of the scaffold. White arrows indicate osteoblasts. Black bars indicate 300 μm.

of these structures, the bioceramics were also vacuum-coated with alginate. This inclusion greatly enhanced both the mechanical and biological properties of the scaffolds. In fact, osteoblast adhesion, migration and proliferation in contact with the coated scaffolds emphasize their suitability for regenerative medicine. To the best of our knowledge this was the first time that this combination of these biomaterials was used to manufacture 3D porous scaffolds, which resulted in unique structures with desirable biological, mechanical and physical properties that will promote bone regeneration. In a near future these hybrid bioceramic–polymeric composites will be implanted in whole animal models with small and large bone defects, in order to evaluate their bone regenerative performance.

Table 3
Summary of physicochemical and biological properties of the manufactured scaffolds.

Properties scaffold	Hydrophilicity	Porosity	Mechanical strength	Biocompatibility
80/20	+	++++++	+++++	+++++
80/20/A	++++	+++++	++++++	++++++
90/10	++	++++	+++	+
90/10/A	+++++	+++	++++	++
99/1	+++	++	++	+++
99/1/A	++++++	+	+	++++

"+" to "++++++": symbol-based grade, indicating improvement of the scaffolds properties.

5. Acknowledgments

The authors would like to thank to Eng. Ana Paula for her help with the acquisition of SEM data. This work was supported by the Portuguese Foundation for Science and Technology (FCT) (PTDC/EME-TME/103375/2008, PTDC/EBB-BIO/114320/2009 and PEst-C/SAU/UI0709/2011 COMPETE). Vítor M. Gaspar acknowledges a PhD fellowship from FCT (SFRH/BD/80402/2011).

Appendix A. Supplementary data

Supplementary data to this article can be found online at http://dx.doi.org/10.1016/j.msec.2013.07.003.

References

[1] A.M. Martins, C.M. Alves, F.K. Kasper, A.G. Mikos, R.L. Reis, J. Mater. Chem. 20 (2010) 1638–1645.
[2] D. Fisher, J. Wong, C. Crowley, W. Khan, Curr. Stem Cell Res. Ther. 8 (2013) 243–252.
[3] T. Jiang, S.P. Nukavarapu, M. Deng, E. Jabbarzadeh, M.D. Kofron, S.B. Doty, W.I. Abdel-Fattah, C.T. Laurencin, Acta Biomater. 6 (2010) 3457–3470.

[4] A. Nekora-Azak, G. Evlioglu, M. Ozdemir-Karatas, H. Keskin, J. Oral Rehabil. 32 (2005) 693–695.
[5] M.B. Dreifke, N.A. Ebraheim, A.C. Jayasuriya, J. Biomed. Mater. Res. A (2013).
[6] A.A. Amini, L.S. Nair, Biomed. Mater. 7 (2012) 024105.
[7] J.R. Jones, L.M. Ehrenfried, L.L. Hench, Biomaterials 27 (2006) 964–973.
[8] D.F. Williams, Biomaterials 29 (2008) 2941–2953.
[9] S. Scaglione, C. Ilengo, M. Fato, R. Quarto, Tissue Eng. Part A 15 (2009) 155–163.
[10] M.G. Raucci, V. Guarino, L. Ambrosio, J. Funct. Biomater. 3 (2012) 688–705.
[11] H.S. Yu, G.Z. Jin, J.E. Won, I. Wall, H.W. Kim, J. Biomed. Mater. Res. A 100 (2012) 2431–2440.
[12] A. Abdal-hay, F.A. Sheikh, J.K. Lim, Colloids Surf. B Biointerfaces 102 (2013) 635–643.
[13] P.P. Cortez, M.A. Silva, M. Santos, P. Armada-da-Silva, A. Afonso, M.A. Lopes, J.D. Santos, A.C. Mauricio, J. Biomater. Appl. 27 (2012) 201–217.
[14] X. Lu, S. Li, J. Zhang, Z. Zhang, B. Lu, H. Bu, Y. Li, J. Cheng, Sheng Wu Yi Xue Gong Cheng Xue Za Zhi 18 (2001) 497–499.
[15] C.F.L. Santos, A.P. Silva, L. Lopes, I. Pires, I.J. Correia, Mater. Sci. Eng. C 32 (2012) 1293–1298.
[16] L.L. Hench, Biomaterials 19 (1998) 1419–1423.
[17] L.L. Hench, J. Biomed. Mater. Res. 41 (1998) 511–518.
[18] C. Wu, Y. Ramaswamy, P. Boughton, H. Zreiqat, Acta Biomater. 4 (2008) 343–353.
[19] Y. Zhang, M. Zhang, J. Biomed. Mater. Res. 61 (2002) 1–8.
[20] S.J. Florczyk, M. Leung, S. Jana, Z. Li, N. Bhattarai, J.I. Huang, R.A. Hopper, M. Zhang, J. Biomed. Mater. Res. A 100 (2012) 3408–3415.
[21] W. TheinHan, M.D. Weir, C.G. Simon, H.H. Xu, J. Tissue Eng. Regen. Med. (2012), http://dx.doi.org/10.1002/term.1466.
[22] W.R. Gombotz, S.F. Wee, Adv. Drug Deliv. Rev. 31 (1998) 267–285.
[23] J.-K. Francis Suh, H.W. Matthew, Biomaterials 21 (2000) 2589–2598.
[24] F.A. Johnson, D.Q. Craig, A.D. Mercer, J. Pharm. Pharmacol. 49 (1997) 639–643.
[25] A.D. Augst, H.J. Kong, D.J. Mooney, Macromol. Biosci. 6 (2006) 623–633.
[26] J.F.A. Valente, V.M. Gaspar, B.P. Antunes, P. Countinho, I.J. Correia, Polymer 54 (2013) 5–15.
[27] O. Smidsrød, Trends Biotechnol. 8 (1990) 71–78.
[28] A.I. Pravdyuk, Y.A. Petrenko, B.J. Fuller, A.Y. Petrenko, Cryobiology 66 (2013) 215–222.
[29] A. Schoubben, P. Blasi, S. Giovagnoli, L. Perioli, C. Rossi, M. Ricci, Eur. J. Pharm. Sci. 36 (2009) 226–234.
[30] X. Wu, Y. Liu, X. Li, P. Wen, Y. Zhang, Y. Long, X. Wang, Y. Guo, F. Xing, J. Gao, Acta Biomater. 6 (2010) 1167–1177.
[31] M. Ebrahimi, P. Pripatnanont, N. Monmaturapoj, S. Suttapreyasri, J. Biomed. Mater. Res. A 100 (2012) 2260–2268.
[32] D. Lacroix, A. Chateau, M.P. Ginebra, J.A. Planell, Biomaterials 27 (2006) 5326–5334.
[33] J. Martin Bland, D. Altman, Lancet 327 (1986) 307–310.
[34] H.L. Nie, L.M. Zhu, Int. J. Biol. Macromol. 40 (2007) 261–267.
[35] M. Rouahi, O. Gallet, E. Champion, J. Dentzer, P. Hardouin, K. Anselme, J. Biomed. Mater. Res. A 78 (2006) 222–235.
[36] T.J. Collins, Biotechniques 43 (2007) 25–30.
[37] P. Coimbra, P. Ferreira, H. De Sousa, P. Batista, M. Rodrigues, I. Correia, M. Gil, Int. J. Biol. Macromol. 48 (2011) 112–118.
[38] V. Bewick, L. Cheek, J. Ball, Crit. Care 8 (2004) 130–136.
[39] A. Hilton, R.A. Armstrong, Microbiologist 2006 (2006) 34–36.
[40] Z. Artzi, M. Weinreb, G. Carmeli, R. Lev-Dor, M. Dard, C.E. Nemcovsky, Clin. Oral. Implants Res. 19 (2008) 686–692.
[41] J.L. Rouvillain, F. Lavalle, H. Pascal-Mousselard, Y. Catonne, G. Daculsi, Knee 16 (2009) 392–397.
[42] V. Wang, G. Misra, B. Amsden, J. Mater. Sci. Mater. Med. 19 (2008) 2145–2155.
[43] M. Xie, M.O. Olderoy, J.P. Andreassen, S.M. Selbach, B.L. Strand, P. Sikorski, Acta Biomater. 6 (2010) 3665–3675.
[44] M.A.A. Muhamad Nor, L.C. Hong, Z. Arifin Ahmad, H. Md Akil, J. Mater. Process. Technol. 207 (2008) 235–239.
[45] H. Fu, Q. Fu, N. Zhou, W. Huang, M.N. Rahaman, D. Wang, X. Liu, Mater. Sci. Eng. C 29 (2009) 2275–2281.
[46] Q. Fu, M.N. Rahaman, B. Sonny Bal, R.F. Brown, D.E. Day, Acta Biomater. 4 (2008) 1854–1864.
[47] B.G. Gerberich, S.K. Bhatia, Biotechnol. J. 8 (2013) 73–84.
[48] R.A. Gittens, T. McLachlan, R. Olivares-Navarrete, Y. Cai, S. Berner, R. Tannenbaum, Z. Schwartz, K.H. Sandhage, B.D. Boyan, Biomaterials 32 (2011) 3395–3403.
[49] C.M. Murphy, M.G. Haugh, F.J. O'Brien, Biomaterials 31 (2010) 461–466.
[50] Y. Zhang, M. Zhang, J. Biomed. Mater. Res. 55 (2001) 304–312.
[51] V. Karageorgiou, D. Kaplan, Biomaterials 26 (2005) 5474–5491.
[52] A. Tampieri, G. Celotti, S. Sprio, A. Delcogliano, S. Franzese, Biomaterials 22 (2001) 1365–1370.
[53] P. Habibovic, M.C. Kruyt, M.V. Juhl, S. Clyens, R. Martinetti, L. Dolcini, N. Theilgaard, C.A. van Blitterswijk, J. Orthop. Res. 26 (2008) 1363–1370.
[54] G. Muralithran, S. Ramesh, Ceram. Int. 26 (2000) 221–230.
[55] A. Balakrishnan, P. Pizette, C. Martin, S. Joshi, B. Saha, Acta Mater. 58 (2010) 802–812.
[56] I. Sopyan, J. Kaur, Ceram. Int. 35 (2009) 3161–3168.
[57] F.C. den Boer, B.W. Wippermann, T.J. Blokhuis, P. Patka, F.C. Bakker, H.J. Haarman, J. Orthop. Res. 21 (2003) 521–528.
[58] H.W. Kim, S.Y. Shin, H.E. Kim, Y.M. Lee, C.P. Chung, H.H. Lee, I.C. Rhyu, J. Biomater. Appl. 22 (2008) 485–504.
[59] M. Okamoto, Y. Dohi, H. Ohgushi, H. Shimaoka, M. Ikeuchi, A. Matsushima, K. Yonemasu, H. Hosoi, J. Mater. Sci. Mater. Med. 17 (2006) 327–336.
[60] J.P. Gleeson, N.A. Plunkett, F.J. O'Brien, Eur. Cell Mater. 20 (2010) 218–230.
[61] Y.C. Chen, R.Z. Lin, H. Qi, Y. Yang, H. Bae, J.M. Melero-Martin, A. Khademhosseini, Adv. Funct. Mater. 22 (2012) 2027–2039.
[62] M.A. LeRoux, F. Guilak, L.A. Setton, J. Biomed. Mater. Res. 47 (1999) 46–53.
[63] T. Shiota, M. Shibata, K. Yasuda, Y. Matsuo, J. Ceram. Soc. Jpn. 116 (2008) 1002–1005.
[64] D.W. Hutmacher, J.T. Schantz, C.X. Lam, K.C. Tan, T.C. Lim, J. Tissue Eng. Regen. Med. 1 (2007) 245–260.
[65] D.N. Rockwood, E.S. Gil, S.H. Park, J.A. Kluge, W. Grayson, S. Bhumiratana, R. Rajkhowa, X. Wang, S.J. Kim, G. Vunjak-Novakovic, D.L. Kaplan, Acta Biomater. 7 (2011) 144–151.
[66] S. Kashef, A. Asgari, T.B. Hilditch, W. Yan, V.K. Goel, P.D. Hodgson, Mater. Sci. Eng., A 527 (2010) 7689–7693.
[67] A. Ślósarczyk, Z. Paszkiewicz, C. Paluszkiewicz, J. Mol. Struct. 744–747 (2005) 657–661.
[68] Z. Dong, Y. Li, Q. Zou, Appl. Surf. Sci. 255 (2009) 6087–6091.
[69] G.S. Lee, J.H. Park, U.S. Shin, H.W. Kim, Acta Biomater. 7 (2011) 3178–3186.
[70] P.H. Warnke, H. Seitz, F. Warnke, S.T. Becker, S. Sivananthan, E. Sherry, Q. Liu, J. Wiltfang, T. Douglas, J. Biomed. Mater. Res. B Appl. Biomater. 93 (2010) 212–217.